

Kinetic and Continuum Modeling of High Temperature Relaxation of O₂ and N₂ Binary Mixtures

Sergey F. Gimelshein* and Ingrid J. Wysong[†]
AFRL, Edwards AFB, CA 93524

Alexander J. Fangman[‡] and Daniil A. Andrienko[§]
Texas A&M University, 710 Ross St., College Station, TX 77840, USA

Olga V. Kunova[¶] and Elena V. Kustova^{||}
Saint Petersburg State University, 7/9 Universitetskaya nab., St. Petersburg 199034, Russia

Catarina Garbacz^{**} and Marco Fossati^{††}
Aerospace Centre, University of Strathclyde, Glasgow, G1 1XJ, United Kingdom

Kyle Hanquist^{‡‡}
University of Arizona, 1130 N. Mountain Ave., Tucson, AZ 85721, USA

The present paper provides a comprehensive comparative analysis of thermochemistry models of various fidelity levels developed in leading research groups around the world. Fully kinetic, hybrid kinetic-continuum, and fully continuum approaches are applied to analyze parameters of hypersonic flows starting from the revision of single-temperature rate constants up to the application in 1D post-shock conditions. Comparison of state-specific and two-temperature approaches show there are very significant and often qualitative differences in the time-dependent nonequilibrium reaction rates and their ratio to the corresponding single-temperature rates. A major impact of the vibration-dissociation coupling on the temporal relaxation of gas properties is shown. For instance, the legacy Park's model has a strongly non-linear behavior of nonequilibrium reaction rate with vibrational temperature, while a nearly linear shape exists for all state-specific approaches. Analysis of vibrational level populations in the nonequilibrium region show a profound impact of the numerical approach and the model on the population ratios, and thus vibrational temperatures inferred from such ratios. The difference in the UV absorption coefficients, calculated by a temperature-based spectral code using vibrational populations from state-specific and kinetic approaches, is found to exceed an

* Aerospace Engineer, Jacobs Technology, gimel@particlematters.inc

[†] Branch Chief, Combustion Devices Branch, AIAA Associate Fellow, ingrid.wysong@us.af.mil

[‡] Ph.D. candidate, Department of Aerospace Engineering, afangman@tamu.edu

[§] Assistant Professor, Department of Aerospace Engineering, daniila@tamu.edu, AIAA Member

[¶] Senior researcher, Fluid Dynamics Dept., kunova.olga@gmail.com

^{||} Professor, head of Fluid Dynamics Dept., e.kustova@spbu.ru

^{**} PhD student, Department Mechanical and Aerospace Engineering, AIAA Member, ana.gomes@strath.ac.uk.

^{††} Associate Professor, Department Mechanical and Aerospace Engineering, AIAA Member, marco.fossati@strath.ac.uk.

^{‡‡} Assistant Professor Dept. of Aerospace and Mechanical Engineering, AIAA Member, hanquist@arizona.edu

order of magnitude.

I. Introduction

Numerical modeling of high temperature nonequilibrium air flows traditionally has been a challenging task, with significant uncertainties attributed to thermal and chemical effects related to high energy collisions in the gas phase and at the surface. Fast relaxation of the internal energy modes, resulting in differences in the mode temperatures and, in the general case, nonequilibrium energy distributions, and thus thermal nonequilibrium, proceeds simultaneously with chemical processes, where unbalanced chemical reactions create strong chemical nonequilibrium. Typically, the excitation of vibrational degrees of freedom and dissociation of oxygen and nitrogen molecules results in a significant decrease in gas temperature in the hot layer of gas between the shock wave and the surface. This, in turn, affects flow observables, such as UV emissions, as well as surface properties, such as distributed heat fluxes. It was shown that predicted surface properties, primarily heat flux, are sensitive to the finite-rate chemistry modeling [1] and, to a lesser extent, thermal nonequilibrium modeling [2]. Several experimental campaigns [3–6] have been conducted over the last two decades to study nonequilibrium flows, aimed at providing surface and flow properties to the modelers, and thus building a reference database for validation of numerical approaches and models. While successful in many aspects, these efforts fell short of providing conclusive datasets that would define key excitation and reaction processes [7]. Today, there is still a considerable level of uncertainty not only related to nonequilibrium rates and the interaction between these processes, but often even in single-temperature rates.

There are a number of reasons for the lack of consensus among modelers on what rates and models to use in each specific case. As described in Ref. [7], the main set of measurements from the 60's and 70's had unknown degrees of vibrational nonequilibrium, and the rates inferred from them had to rely on semi-empirical models for interpretation. They also have considerable scatter and variation amongst the results. Validation of reaction rates from heat flux measurements is not possible due to the complex set of processes that contribute to the measurable quantity, as well as to the often unknown uncertainty in freestream conditions. Comprehensive uncertainty quantification studies, such as Refs. [8, 9], are a robust tool that is expected to help design and interpret improved experimental studies.

The above problems have been recognized by the research community, and remarkable progress has been made over the last few years toward improving the accuracy of numerical analysis of high temperature nonequilibrium air flows. Both theoretical and experimental work contributed to this progress. The development of accurate potential energy surfaces for oxygen and nitrogen collisions, and the use of those surfaces in parametric quasiclassical trajectory (QCT) calculations, made available high-fidelity state-specific rates and detailed cross-sections for internal energy excitation, dissociation, and exchange reactions in key collision paths [10, 11]. Increasing accuracy and relevance of conditions in experimental studies, primarily those currently conducted in shock tubes, with both incident [6] and reflected [12–15] shock configurations, and in hypervelocity wind tunnel and expansion tube facilities [16, 17], all promise to offer

reliable data with error bars significantly lower than those of past experiments. These theoretical and experimental achievements, as was argued in our earlier work [18], may provide a solid basis and motivation for adopting a common set of benchmark cases in the nonequilibrium CFD community, similar to GEC RF Reference Cell in the plasma physics community [19].

A small step in this direction was made in Ref. [18], where Hypersonic NonEquilibrium Comparison Cases (HyNECC) for nonequilibrium CFD methods were introduced (see also www.github.com/hynecc). The HyNECC cases will be the first steps toward a needed benchmarking and validation effort that can be envisioned in the long term as including:

- 1) Comparison of reaction and relaxation rates produced by different models and implementations at (i) equilibrium, (ii) two- or three-temperature nonequilibrium regimes, and (iii) the quasi-steady-state (QSS).
- 2) Projecting the differences and similarities in models and rates onto realistic nonequilibrium hypersonic flow conditions.
- 3) Comparison with available experimental data in order to understand how well or poorly state-of-the-art models predict flow properties.
- 4) Finding properties and conditions most indicative and most sensitive to models, parameters, and implementations.
- 5) Providing specific feedback to the experimental community on conditions, properties, and flows of interest.
- 6) Establishment of a clear and straightforward set of benchmarks for future code and model development.

These are difficult and demanding tasks; each of them requires a dedicated effort and cooperation from the research community. The initial test set proposed in Ref. [18] included several fixed-temperature and isothermal heat bath conditions in pure nitrogen and oxygen; however, this was later expanded to include adiabatic heat bath relaxation in air, one-dimensional shock wave, and a two-dimensional airflow over a double cone (the latter was later replaced by a flow over a cylinder). The challenging nature of the effort was manifested in our preliminary study of adiabatic heat bath relaxation of air, which essentially was the first step toward HyNECC development. An example of obtained results is shown in Fig. 1, where the time relaxation of nitric oxide mole fraction is shown. To reproduce typical conditions behind a shock wave in a hypersonic flow, the initial translational and rotational temperatures were set to $T_{trn} = T_{rot} = 15,000$ K, the initial vibrational temperature was $T_{vib} = 300$ K, and initial gas composition was 79% N_2 and 21% O_2 . Here, SPARTA [20] and SMILE [21] are DSMC codes, US3D [22] is a two-temperature Navier-Stokes code, and STS [23] is a state-to-state continuum solver discussed below. LB, FHO, FHO-FR stand for Larsen-Borgnakke [24], Forced Harmonic Oscillator [25], and Forced Harmonic Oscillator - Free Rotator [26] models of the vibration-translation energy transfer, respectively. TCE (total collision energy), Bias, Park, MMT, Saveliev, and Starik stand for models [23, 27–31] of chemical reactions, respectively. The use of different codes, methods, models, and rates in each of these calculations lead to the situation where virtually all results differ, and it is hard to draw any meaningful conclusions except that numerical studies clarifying the reasons for such differences are needed, as are

experimental data sets as discussed earlier.

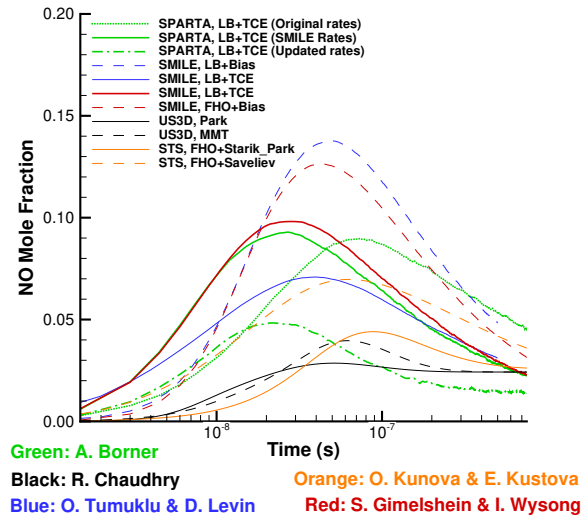


Fig. 1 Nitric oxide mole fraction in an adiabatic heat bath reactor at 15,000 K.

Any attempt to quantitatively explain the lack of agreement in macroscopic properties obtained by different approaches to modeling high-temperature adiabatic air relaxation will be complicated by the fact that there are many thermal and chemical processes that impact different gas properties simultaneously. With that in mind, the authors of this work chose to begin with a smaller problem, reducing behind-the-shock adiabatic air relaxation to that of binary oxygen and nitrogen mixtures. In each of these cases, there are only two dissociation reactions and two vibration-translation (VT) energy transfer channels. These processes play a significant role in air relaxation, and thus understanding expected differences would be the first step toward the analysis of five-species air relaxation. It is important to point out that there are three primary contributors to such differences:

- Numerical approach. While any nonequilibrium flow solver may be considered to some extent as an approximate solution of the Boltzmann equation, the level of approximation differs considerably. For example, the direct simulation Monte Carlo (DSMC) method [27] takes into account all levels of flow nonequilibrium: translational, rotational, vibrational, electronic, and chemical. It may rely, however, on empirical models for many thermal and chemical processes [2]. The level of detail in the description of vibrational and chemical relaxation may be much higher when the vibrationally resolved, QCT-based master equation [32] is used; this approach is somewhat cost-prohibitive in 2D flowfields [33], but the ultra-simplified zero-dimensional bath case is well suited for comparing it to other approximations. Recent work [34], however, argues that master equations based purely on vibrational quantum levels which ignore coupling between vibrational and rotational states may have inaccuracies. A continuum approach based on the solution of the Navier-Stokes (NS) equations trades the assumption of small deviations from equilibrium for a drastic increase in computational efficiency. The traditional single-temperature

approximation of NS may still be refined by the separation of vibrational and translational-rotational temperatures [29], and even further, with a state-to-state approach [23, 35, 36].

- Single-temperature reaction and relaxation rates. These rates are arguably the most important aspect which explicitly changes the temporal relaxation of gas properties. Direct comparison of rate dependence on temperature is fairly straightforward in equilibrium conditions, but the adaptation of prescribed rates, and precise matching of rates used by different approaches, is not. Some methods may reproduce, or explicitly impose, temperature-dependent rate constants, such as those derived from experimental data and often presented in the Arrhenius format. However, many state-specific approaches, both kinetic and continuum, use energy-dependent collision cross-sections or temperature-dependent state-specific rates with some physical constraints. In this case, temperature-dependent rate constants are the product, and not the input, of the approach.
- Nonequilibrium models. This part, and the contributions related to it, are traditionally associated with large uncertainty. This is often due to the scarcity of information used to build such models, or the difficulty in adapting energy-dependent information in cases where it is available, such as massive QCT databases for some of the air species collision types. Within a single numerical approach, one can often use different nonequilibrium models that reproduce the same, or nearly the same, single-temperature rates. The results, however, will differ in parts of the flow where thermal nonequilibrium, be it at the level of energy distributions, or difference in the energy mode temperature, is significant.

To examine all three contributors, we have used here various continuum and kinetic nonequilibrium solvers with four different numerical approaches, as detailed below. The starting point for each approach is to use their baseline, “best guess”, rates and models. This is then followed by changing rates and, where necessary and possible, rate matching. Then, the impact of models is analyzed for each of the approaches. Possible implications related to the use of QCT and data-based rates are examined in heat bath and reflected shock settings. While both nitrogen and oxygen adiabatic heat baths are considered in this work, somewhat more attention is paid to oxygen. This is because experimental data on oxygen relaxation is more readily available at this time [12], and oxygen is also the primary focus of hypersonics diagnostics currently being pursued [14, 17].

II. Flow conditions

The two baseline flow conditions considered in this work are spatially homogeneous oxygen and nitrogen adiabatic heat baths. For oxygen, the gas is initially pure O_2 , with translational and rotational temperatures of $T_{trn} = T_{rot} = 10,000$ K, and a vibrational temperature of $T_{vib} = 300$ K. The gas is then relaxed adiabatically through thermal energy transfer and two dissociation-recombination reactions: $O_2+O_2 \leftrightarrow O_2+O+O$ and $O_2+O \leftrightarrow O+O+O$. For the nitrogen bath, the initial translational and rotational temperatures of N_2 are set to 20,000 K; similar to oxygen, two dissociation-recombination reactions are modeled. In both cases, the initial number density is 10^{25} molecule/m³. No ionization reactions are

considered, but electronic excitation is included in some cases, as discussed below. In cases where it is included, the initial electronic temperature of 300 K is assumed. Different initial temperatures are set in these baths in order to obtain a similar level of flow nonequilibrium at comparable relaxation times.

It has to be noted here that the above number density is significantly higher than that of a typical free stream in a medium to high altitude flight or in its high-enthalpy ground facility equivalent. As the result, the characteristic relaxation time scales in the corresponding thermal baths are in nanoseconds to microseconds, instead of conventional microseconds to milliseconds observed in hypersonic nonequilibrium flows. The primary reason for choosing such a high density in this work is that it allows one to examine in detail both the molecular dissociation and exchange reaction dominated relaxation, where the translational and rotational temperatures drop significantly from their after-shock values, and the atom-recombination dominated relaxation where the gas cools down, and approaches the equilibrium (thermal and chemical) steady state. Using a lower density significantly increases the time to reach steady state, and a significant enough reduction would make computations impractical for the most time consuming approach used here, the DSMC method. It is important to note that increasing the initial gas density does not change the applicability of the results to hypersonics. This is because the key thermal and reactive processes inside and behind the bow shock in front of a spacecraft or a test body are binary collisions driven, and thus the relaxation times simply scale with gas density. Furthermore, the gas density used here is close to that typically observed in the very vicinity of the cold surface in an experimental setting, such as, for example, HEG-III test condition measured in Ref. [4], where the gas number density along the stagnation streamline peaked at about 10^{25} m^{-3} near the cold wall. Three-body recombination reaction rates are usually weak functions of temperature, and thus the last part of the relaxation shown here is believed to reasonably approximate that of cold-wall experimental or flight conditions with a free stream gas density on the order of 3 g/m^3 .

Another flow condition, which is simulated here only with the DSMC method, was inspired by the success of recent measurements of vibrational relaxation times and dissociation rates in oxygen and air relaxing behind strong reflected shock waves [14]. This work presents the results of time accurate numerical simulations of incident shock waves propagating at a velocity of 2.8 km/s through stagnant oxygen gas kept at a pressure and temperature of 40 Pa and 296 K, respectively. The objective of this modeling is to establish what the impact of using the best available QCT- and experimental-based thermal and reaction rates is, and whether the difference between them is larger than a typical experimental error bar [14], and thus detectable.

III. Numerical Approaches and Physical Models

Summary of major parameters of all five models under consideration is given in Table 1.

Name	Source of VT model	Source of chemistry model	Detailed balance
DSMC [21]	State-sampled, high-fidelity: LB, 3D FHO-FR[26], fitted to QCT data [37, 38]	high-fidelity: Extended Bias [40] low-fidelity: TCE[2, 41]	Gibbs free energy [42]
	low-fidelity: LB, Park[39]		
ME [43]	State-resolved QCT[44–47]	State-resolved QCT [44–47]	Partition function based
STS [48]	State-resolved FHO [49]	Modified Marrone–Treanor model [50]	Partition function based
		fitted to QCT data [51, 52] (N ₂ -N, O ₂ -O) and [53] (O ₂ -O ₂ , N ₂ -N ₂)	
SU2-NEMO [54]	Landau-Teller [55]	Two-temperature, Park [56, 57]	Gibbs free energy [57]
LeMANS [58, 59]	Landau-Teller [55]	Two-temperature, Park [56]	Gibbs free energy [60]

Table 1 Summary of models

A. DSMC method

The direct simulation Monte Carlo (DSMC) method [27] is used as the fully kinetic approach. It is applied here to model the spatially uniform adiabatic heat bath relaxation cases and a one-dimensional reflected shock wave. All DSMC simulations shown in this work are performed with the SMILE [21] code. The variable hard sphere model [41] is applied with interaction parameters listed in Table II of Ref. [2], calculated from the viscosity-temperature data of Ref. [61]. The internal energy modes are discrete, both rotational and vibrational. The Larsen-Borgnakke model [24] for discrete energy levels [62] is used to compute the rotation-translation energy transfer. For the vibrational energy transfer and chemical reactions, both a higher fidelity and a lower fidelity model are used.

In the high-fidelity model, chosen in this work as the baseline, the state-to-state 3D Forced Harmonic Oscillator - Free Rotator (FHO-FR) [26] model is used for vibration-translation energy transfer in molecule-molecule collisions, with the DSMC implementation discussed earlier [63]. The discrete Larsen-Borgnakke (LB) model [64] is used to simulate the vibration-translation energy exchange in molecule-atom collisions, with temperature-dependent vibrational collision numbers based on QCT calculations [37], along with a DSMC correction [38]. Vibration-vibration energy transfer is modeled with the empirical near-resonant approach [65]. The extended Bias model [28, 66] is used for dissociation and recombination reactions, with parameters given in Ref. [40].

In the low-fidelity model, the vibration-translation energy transfer for molecule-molecule collisions is performed with the LB method using the vibrational collision numbers based on the semi-empirical Millikan-White correlation [55] with Park’s high-temperature correction [39]; the vibration-vibration transfer was not taken into account. The total collision energy (TCE) model [41] was used for all reactions, with reaction rates at equilibrium reproducing those of the Bias model [2]. The reaction rate constants used in this work are summarized in Table 2 of [2].

B. Master Equation (ME) model

The ME model is a high-fidelity thermochemistry model that combines the accuracy of the kinetic simulations and the efficiency of the continuum approach. Kinetic data in the ME approach is obtained via the QCT method. A system of master equations, similar to that of the STS model in the next section, allows for fast integration of governing equations in time with variable time-stepping and error control. Potential energy surfaces employed in the present work are of the highest accuracy currently available in the open literature.

QCT trajectories are initialized with rotational states sampled according to Boltzmann statistics. The initial vibrational state of the target species is fixed for each trajectory batch and runs from the ground to the final state before the dissociation limit. The O₂ and N₂ energy ladders contain 44 and 60 vibrational states respectively. Collision energies between target species (O₂ or N₂) and projectile species (O, N₂, or O₂) range between 0.05 and 10 eV. QCT simulation of the O₂-O system includes all 9 PESs that correlate with the O₃ ground electronic state [45]. O₂-O₂ and N₂-N₂ rate coefficients are obtained on the triplet O₄ PES [44] and singlet N₄ PES [47]. To avoid modeling low probability events (i.e. collisions between two molecules in excited vibrational states), the initial vibrational state of molecular projectiles is given by the ground and first vibrational states only. N₂-N kinetic data is taken from the NASA Ames database and interpolated on the present vibrational ladder [46].

Overall, the kinetic database comprises approximately 10 billion trajectories across 10 translational-rotational temperatures between 2,000 K and 20,000 K. The database includes rate coefficients of inelastic, exchange, swap-dissociation, double-swap, direct dissociation, and double dissociation channels [67]. The original rate coefficients are resolved with respect to the initial and final vibrational states of the molecular reactants and products; however, the database is reduced to reflect specifics of energy exchange at hypersonic temperatures. Under present conditions, vibration-vibration energy transfer in pure gases is of minor importance, and bound-bound transitions are primarily governed by the vibration-translation energy exchange. For this reason, vibration-vibration energy transfer is neglected, and the bound-bound rate coefficients are reduced to the form $K_{v \rightarrow v'}$, where v and v' are the initial and final vibrational states respectively.

A system of master equations describing the temporal evolution of the number density of vibrational states and atomic species is constructed. This set of coupled ordinary differential equations is integrated from an initial thermally nonequilibrium state. For the system including both molecule-molecule and molecule-atom interactions, the master equations take the following form:

$$\begin{aligned} \frac{dn_v}{dt} = & \sum_{v \neq v'} \left(K_{v' \rightarrow v}^{M-A} n_A n_{v'} - K_{v \rightarrow v'}^{M-A} n_A n_v + K_{v' \rightarrow v}^{M-M} n_M n_{v'} - K_{v \rightarrow v'}^{M-M} n_M n_v \right) \\ & + R_v^{M-A} n_A^3 - D_v^{M-A} n_v n_A + R_v^{M-M} n_M n_A^2 - D_v^{M-M} n_v n_M, \quad v = 0 \dots v_{max} \end{aligned}$$

where K , D , R are the rate coefficients of bound-bound, dissociation and recombination transitions, superscripts $M - M$ and $M - A$ designate molecule-molecule and molecule-atom interactions, and subscripts $v \rightarrow v'$ and $v \rightarrow c$ refer to vibrationally-resolved bound-bound and bound-free transitions. A single simulation of an adiabatic relaxation case takes 2 core-min.

C. State-to-state (STS) approach

One of the continuum approaches suitable for modeling strongly nonequilibrium flows is the state-to-state model [68]. It is based on the assumption of completely coupled chemical reactions and vibrational energy transitions (rovibrational in more advanced models [43, 69]). In the state-to-state (STS) approach, the fluid dynamic equations are coupled to the master equations for internal state populations; the production terms in these equations depend on the state-resolved rate coefficients of chemical reactions and internal energy transitions.

The STS model is discussed in detail in [48]. Here it is applied for spatially homogeneous adiabatic heat bath simulations. The vibrational energies are described by an anharmonic oscillator with 68 and 47 states [52, 70] for nitrogen and oxygen molecules, respectively. Single-quantum VT transitions, state-resolved dissociation, and recombination reactions in a collision with a molecule or an atom are taken into account. Rate coefficients of vibrational energy exchanges are calculated using the FHO model [49]. The state-dependent dissociation rate coefficients for molecule-atom interactions are calculated using the generalized Marrone–Treanor model [50] with the sets of parameters evaluated on the basis of QCT data [51, 52]. For molecule-molecule interactions (O_2 - O_2 and N_2 - N_2 collisions), the corresponding constants in the Arrhenius law are taken from [53] and, furthermore, the parameter $U = 3T$ (T is the gas temperature) is used for both reactions. The obtained state-resolved rate coefficients of O_2 - O_2 dissociation are in very good agreement with those used in the ME simulations. The backward reaction rate coefficients are calculated by applying explicitly the detailed balance principle derived from the microscopic reversibility relations. Such an approach is more self-consistent than using the equilibrium constants K_{eq} since the latter take into account electronic excitation, and in our test case, the electronic states are neglected.

Simulations in the STS case are carried out using the Matlab `ode15s` function, which was created for integration of stiff ordinary differential equations. The `ode15s` is a variable-step, variable-order (from 1 to 5) solver based on the numerical differentiation formulas. In the calculations, the absolute and relative error tolerances are set equal to 10^{-8} , which gives high accuracy at low time costs.

D. CFD Approaches - 2T Model

CFD approaches are also used to model the zero-dimensional adiabatic heat bath relaxation. The two codes utilized are the open-source SU2-NEMO [54] (NonEquilibrium MOdels) code and LeMANS code [58, 59]. Thermochemistry models are implemented into SU2-NEMO via linking to the Mutation++ library [71] (Multicomponent Thermodynamic

And Transport properties for IONized gases in C++), which provides algorithms for the computation of thermodynamic and chemical kinetic gas properties. LeMANS was developed as a CFD code with a focus on thermochemical nonequilibrium capabilities. The two codes are included here to provide a comparison between different solvers with intricate implementations that are expected to provide similar results. The zero-dimensional test case is modeled by using a 5x5 two-dimensional grid with a symmetry boundary condition applied to all boundaries. In terms of numerical approaches, SU2-NEMO uses a finite-volume edge-based formulation with the AUSM scheme [72], whereas LeMANS uses the finite-volume method with a modified Steger-Warming Flux Vector Splitting scheme [73]. SU2-NEMO uses a second-order backwards-difference discretization to address time evolution while LeMANS used an explicit first-order accurate time integration for these cases. A time step of 1×10^{-10} s is used for both codes to provide detailed time resolution given the relatively low computational cost compared to previous methods discussed.

The physical models used in each of the CFD codes are similar. The two-temperature model by Park [56] is used, where the translational energy mode is assumed to be at equilibrium with the rotational one, and the vibrational energy mode is assumed to be at equilibrium with the electronic one. This assumes that the rotational and translational energy modes of all species can be described by a single temperature, T_{tr} , because the rotational energy equilibrates with the translational energy in just a few collisions. Furthermore, this assumes that the vibrational and electronic energy modes of all species and the electron translational energy mode can be described by another single temperature T_{ve} . The internal mode energies are defined on the basis of the Rigid-Rotor/Harmonic Oscillator model (RRHO). The change in the vibrational energy of the mixture is accounted for as the sum of the vibration-translation energy transfer and energy exchanges due to chemical activity. The rate of energy exchange between the translational and vibrational energy modes follows the Landau-Teller model [74] with the Millikan and White [55] coefficients together with the Park correction [75] for the calculation of relaxation times. The forward reaction rates are defined according to the modified Arrhenius equation, with the controlling temperature determined by Park's two-temperature model [56]. The dissociation reactions are controlled by a combination of the translational-rotational and the vibrational-electron-electronic temperatures ($T_c = T_{tr}^a T_{ve}^b$) to account for the fact that vibrationally excited molecules are more likely to dissociate. This work sets the values of a and b to 0.5. The forward reaction rates are calculated using the Arrhenius curve fits with the controlling temperature, where the reaction rate coefficients are taken from [75, 76]. The backward reaction rates are obtained from the equilibrium constants, as detailed in Refs. [60, 77]. The change in vibrational-electronic energy of the mixture due to the production/destruction of species follows two different models: non-preferential and preferential dissociation models [57]. The former model assumes that molecules dissociate/recombine at the average vibrational energy of the cell, at the given vibrational temperature, whereas the latter accounts for the fact that molecules only dissociate/recombine at higher vibrational levels. In this work, a simple preferential model is used, where the value of energy added or removed is 30% of the dissociation energy. The backward reaction rates are determined from the equilibrium constants, which are calculated as a function of the Gibbs free energy [57]. The primary difference in physical models between the two

codes is how each handles electronic energies. In both codes, the species electronic energy, $e_{el,s}$ is modeled by:

$$e_{el,s} = \begin{cases} \frac{R_{el}}{M_s} \frac{\sum_{i=1}^{\infty} g_{i,s} \theta_{el,i,s} \exp(-\theta_{el,i,s}/T_{ve})}{\sum_{i=1}^{\infty} g_{i,s} \exp(-\theta_{el,i,s}/T_{ve})} & \text{for molecules and atoms,} \\ 0 & \text{for electrons} \end{cases} \quad (1)$$

where $\theta_{el,i,s}$ and $g_{i,s}$ are the characteristic electronic temperature and the degeneracy of the i -th energy level, respectively. This model is utilized because it is accurate for the low electronic energy levels and the energy contribution of the higher levels is negligible [78]. The LeMANS code takes the necessary data from Ref. [58] whereas SU2-NEMO, through Mutation++, and uses the spectroscopic data from the Gurvich tables [79, 80]. Mutation++ uses a pragmatic approach for truncating the partition function by matching the species data of Gurvich using electronic specific data for vibration.

IV. Results and Discussion

A. Equilibrium energy exchange and reaction rates

Results of any nonequilibrium high temperature air flow modeling depend to a large extent on what thermal and chemical rates are imposed, explicitly by direct input or implicitly through models and assumptions. The most straightforward approach for evaluating the importance of rates used in different models is to compare them at equilibrium conditions in the temperature range of interest. In the most general case, this should refer to all collision-related processes that play a role in high temperature air relaxation, starting from transport properties, i.e. viscosity, diffusion, and thermal conduction, to energy transfer between translational, rotational, and vibrational modes, to electronic excitation, and finally, to chemical reactions. The latter refers to binary reactions of dissociation and exchange, three-body collisional recombination, and various ionization processes. Some of these processes are either less important or better known than others, and some are both important and yet still have a significant degree of uncertainty. To the latter group, excitation of vibrational degrees of freedom, dissociation and exchange reactions, and ionization processes are conventionally attributed.

In this work, the main focus is on the collision processes between neutral species, and thus for the binary mixtures considered here, only vibrational excitation and dissociation are considered in detail. Note that while there are several collision channels that impact vibrational relaxation, such as vibration-vibration, vibration-rotation, and vibration-electronic energy transfer, here we only examine the vibration-translation energy transfer, as it has long been known to have a dominant contribution to flow properties [81] when compared to the others, as was shown numerically [82]. In this section, we consider vibrational relaxation times and dissociation rate constants at equilibrium conditions. The e-folding approach [83] is used to evaluate the vibrational relaxation times in flow solvers that do not set that property explicitly (see also the discussion in Ref. [83] regarding the choice of the method to evaluate the vibrational relaxation time). In this case, the gas is kept at a constant translation-rotation temperature T , with no chemical

reactions allowed, and the vibrational energy increases in time from its initial value of 300 K to the final $T_{vib} = T$. The vibrational relaxation time, τ_v , is the time it takes the gas to reach the state when the average vibrational energy of molecules is $E_{vib} = \frac{1}{e}E_{vib,i} + \left(1 - \frac{1}{e}\right)E_{vib,f}$. Here, $E_{vib,i}$ and $E_{vib,f}$ are the initial and final average vibrational energy, respectively. For molecule-molecule collisions, the gas system used to evaluate τ_v includes only these molecules; for molecule-atom collisions, there is only a trace amount of molecules in the system, the rest being atoms.

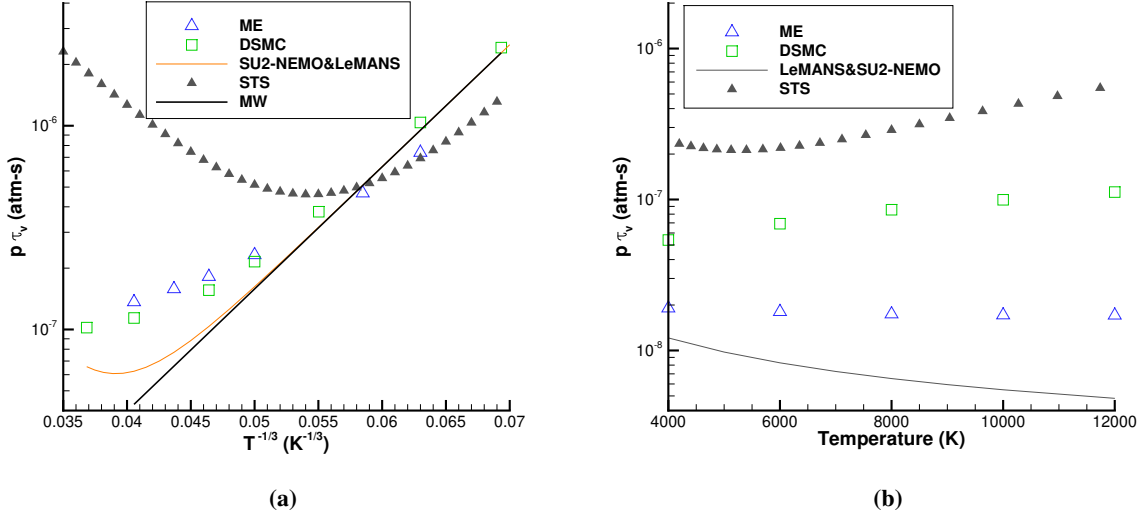


Fig. 2 Vibrational relaxation time for O_2-O_2 (a) and O_2-O (b) collisions.

The vibrational relaxation times used in different flow solvers are presented in Fig. 2a for O_2-O_2 collisions. This interaction type has been studied experimentally and theoretically for more than six decades, and it has been conventionally regarded as one where the well known Millikan and White (MW) [55] semi-empirical correlation is valid, at least for temperatures up to approximately 8,000 K. The key point of the systematics [55] is that the product of the gas pressure, p , and the vibrational relaxation time, τ_v , is a linear function of $T^{-1/3}$. To account for this, the X -axis in Fig. 2a is $T^{-1/3}$. After the publication [55], it was argued that while the linear trend appears correct at a lower temperature, at high temperatures it produces non-physically low vibrational collision times, as it becomes comparable or even lower than the elastic collision time [39]. As a simple remedy to this problem, Park [39] proposed to consider the total vibrational relaxation time in two parts, $\tau_v = \tau_v^{MW} + \tau_v^P$. The first, τ_v^{MW} , is the Millikan-White correlation, while the second, τ_v^P , is a purely empirical correction, often called high-temperature Park's correction. The latter was assumed [39] to be $\tau_v^P = 1/(n\sigma_v c)$, where n and c are the gas number density and thermal velocity, respectively, and $\sigma_v = \sigma_s \left(\frac{50000}{T}\right)^2$, where $\sigma_s = 3 \times 10^{-21} \text{ m}^2$. Note here that a temperature dependence of Ref. [84] derived for an inelastic collision of molecules with an exponential interaction potential was found recently [14] (called Landau-Teller scaling in that work) to provide better agreement with experimental data on VT relaxation of O_2 than MW.

The above MW semi-empirical correlation with the empirical Park's correction is used in both NS solvers, and the comparison with MW clearly indicates a somewhat higher $p\tau_v$, and thus slower relaxation, at higher temperatures. For the temperature conditions considered in this work, however, where the initial oxygen temperature is 10,000 K, the impact of the high temperature correction is expected to be minor. It is also worth noting that the high temperature relaxation is faster in the NS solvers when compared to the state-specific ones. Generally, the use of the Park's correction, or its derivatives, has become standard in two-temperature CFD codes, and is often used in DSMC codes as well. It may, however, require further modification for oxygen collisions based on the most recent measurements [14] and theory.

The Millikan and White correlation has often been applied not only to molecule-molecule interactions, but also to molecule-atom interactions, and many solvers still use it today for collisions such as O_2-O . However, vibrational energy transfer in these collisions differs significantly from those of O_2-O_2 ; one particular reason being the dominant effect of exchange reactions in the vibrational relaxation. For O_2-O , τ_v is not expected to be a linear function of $T^{-1/3}$. Moreover, recent QCT calculations [43, 85] have indicated that $p\tau_v$ may increase with temperature, and not decrease as in O_2-O_2 . The complicating factor in the validation of τ_v for O_2-O is that experimental analysis of this interaction is rather complicated. This is because the vibrational relaxation is affected by several thermal and chemical processes simultaneously, making error bars very significant (see, for example, the discussion in Ref. [6]). The comparison of $p\tau_v$ used in four different solvers is given in Fig. 2b. Here, the NS solvers follow the conventional MW expression, while both ME and DSMC are based on QCT results, even though from different sources: the present QCT data with the potential energy surface (PES) of Ref. [45], and QCT calculations [37] with PES [86], respectively. One can see that there is a large difference, which exceeds an order of magnitude at higher temperatures. It may be argued that the ME curve is the most accurate because it is based on the most recent QCT/PES results, but a high accuracy experimental input would be necessary to provide final validation. There is, however, very limited experimental data on O_2-O VT relaxation as compared to O_2-O_2 , which makes it difficult to distinguish which model is more accurate, as was discussed previously in Refs. [13, 43].

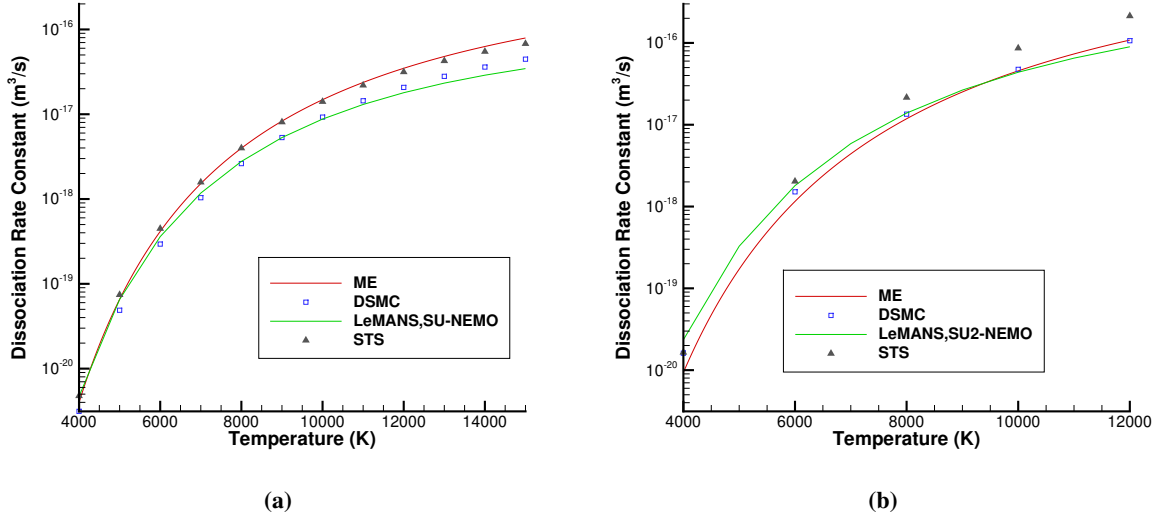


Fig. 3 Dissociation rate constant for O_2-O_2 (a) and O_2-O (b) reactions.

The reaction rate constant for O_2-O_2 dissociation is an important property that controls the atomic oxygen mole fraction during the initial stage of oxygen dissociation. There are a number of experimental and theoretical recommendations for this constant available in the literature (see, for example, Ref. [12] and references therein). Among those, one of the most widely used is the one of Park [87], who derived it by fitting older experimental data on oxygen relaxation behind incident and reflected shocks using his two-temperature model. The sound analysis of Ref. [87] provides reaction rate coefficients that are believed to have relatively low error bars, and thus are still used in many CFD computations. In this work, two flow models rely on Park's rate constants, LeMANS and SU2-NEMO. The corresponding single-temperature rate constants, k_d , at $T_{trn} = T_{rot} = T_{vib}$ are shown in Fig. 3a for O_2-O_2 . The rate constants of DSMC are fairly close to those used in the Navier-Stokes solvers at all temperatures. k_d for ME and STS are close to the others at low temperatures, but approximately a factor of two higher at $T > 10,000$ K. Note that the temperature-dependent reaction rate constants shown here are not imposed in the state-to-state and kinetic approaches, but calculated for the baseline parameters of the reaction model. The latter ones are obtained from fitting energy dependent QCT cross-sections in ME and QCT-based nonequilibrium reaction rates in DSMC. Generally, the agreement at low to moderate temperatures is satisfactory. For higher temperatures, a smaller difference would be preferred but may be hard to achieve due to scarce experimental data in that range and large error bars inherent in such data.

A certain degree of caution is necessary when comparing reaction rate constants deduced from experimental data with those obtained theoretically, such as those based on QCT or quantum mechanical calculations (see also Ref. [14] for a relevant in-depth discussion). For the latter, the rate constants are equilibrium, because equilibrium conditions are easily maintained. However, in an experiment, i.e. a shock tube measurement, such an idealized scenario is not

possible for obvious reasons. The real chemically relaxing gas behind a shock wave is not expected to be at thermal equilibrium because the non-balanced chemical reactions often preferentially impact certain parts of the energy spectrum of colliding molecules, thus resulting in non-Maxwellian velocity distributions and non-Boltzmann internal energy populations. The simplest example here are dissociation reactions which involve oxygen and nitrogen molecules: the reaction cross-sections are many orders of magnitude larger for molecules at higher vibrational levels than for those near the ground vibrational state, even when the total energy of the collision is similar. This process, often called vibrationally favored, or coupled, dissociation, results in a strongly non-Boltzmann vibrational distribution function (VDF) at the so-called quasi-steady-state (QSS) [88]. In this case, the populations of higher vibrational states are depleted, which may happen even when the lower states (and thus the vibrational temperature inferred from those states) are at equilibrium with the rotational and translational energy modes. This causes the dissociation rate to decrease at QSS when compared to equilibrium at the same temperature; that difference may be quite significant, as discussed in Ref. [6, 12]. Such a lower dissociation rate due to a non-Boltzmann VDF is extremely relevant to vibrational state-specific numerical approaches; those that use temperature dependences do not encounter it if their rates are QCT (or other theory) based. The situation is more complex if temperature dependent rate constants are based on experimental data sets, because of the inherent nonequilibrium present in any experiment. Moreover, the populations of excited electronic states may well be significant in an experimental setting, even though they are usually neglected in QCT.

Comparison of single-temperature reaction rate constants for O_2 -O dissociation is presented in Fig. 3b. Similar to the O_2 - O_2 reaction, there is a good agreement between the rate constants obtained in DSMC and those used in the Navier-Stokes solvers. The DSMC slope is somewhat steeper, but the difference does not exceed 20% for all temperatures. The STS rates are again higher than DSMC and NS, while the QCT-based ME predictions are very close to DSMC. Generally, taking into account significant uncertainties related to any experimental estimates of the rate constant for this reaction, it is believed that the agreement between the rate constants associated with different approaches is reasonable.

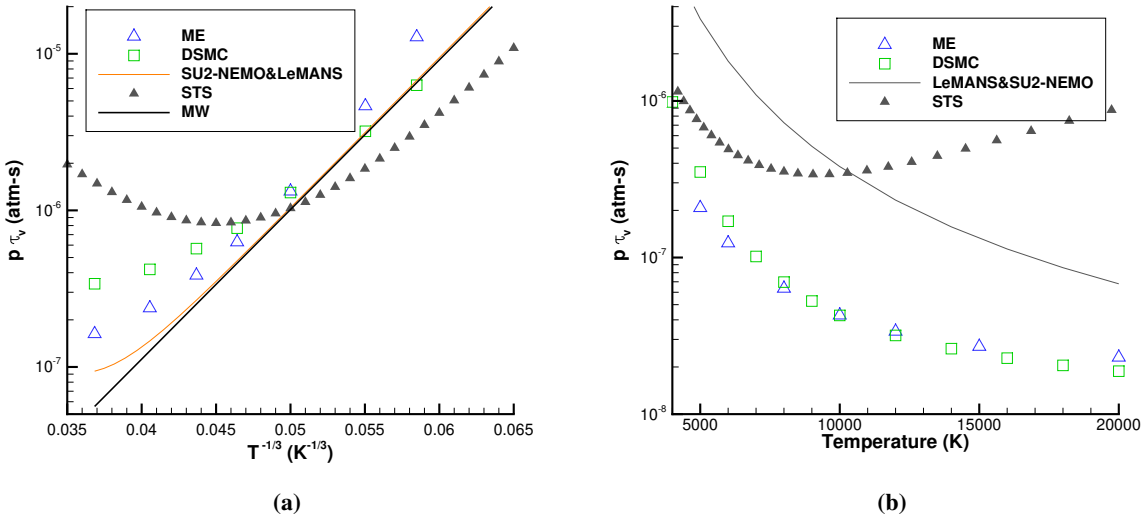


Fig. 4 Vibrational relaxation time for N_2-N_2 (a) and N_2-N (b) collisions.

Consider now the vibrational relaxation times and dissociation rate constants for nitrogen collisions. The values of N_2-N_2 τ_v for different numerical approaches are shown in Fig. 4a. The Millikan and White semi-empirical correlation is also shown here. Again, it is a straight line, as τ_v is assumed to be a linear function of $T^{-1/3}$. Both Navier-Stokes solvers include Park's high-temperature correction to prevent an unphysical increase in the VT rate at higher temperatures. This correction is the same as that for O_2-O_2 collisions (see above). The DSMC τ_v is based on the FHO-FR model, which does not have a free parameter that would control the slope. This FHO-FR slope is noticeably less steep than MW, and the VT relaxation is slower than MW at high temperatures, but approaches MW as the temperature decreases. The STS τ_v , based on the FHO model, has the weakest dependence on temperature, with values at high temperatures approaching those at low temperatures. The vibrational relaxation in ME is faster than in DSMC and STS at high temperatures, but considerably slower at low temperatures. ME arguably may be considered the most accurate here, as it directly relies on recent QCT results based on the potential energy surface in Ref. [47]. It is not clear, however, how accurate the low-temperature trend of ME is, especially keeping in mind increasing error bars of such calculations when T decreases. The QCT method, when coupled to the histogram binning used in the ME model, is known to hinder vibrational relaxation events at low temperatures, which leads to the overestimation of relaxation times visible in Fig. 4. A possible remedy for this situation is the use of Gaussian-weighted binning[89] or semi-classical trajectory methods [90]. Similar to oxygen, the Park's high-temperature correction slows down vibrational relaxation at high temperatures when compared to MW, but the τ_v values for the NS solvers still fall significantly lower than the state-specific approaches. With the known lack of well resolved and accurate experimental data on nitrogen VT relaxation times in that temperature regime, and it may be difficult to assess which τ_v profile provides a better description of real gas.

The vibrational relaxation times for N_2 -N collisions are shown in Fig. 4b. Similar to the oxygen collisions, τ_v is not expected to be a linear function of $T^{-1/3}$, and thus gas temperature is used in the X-axis. There is very good agreement between τ_v , obtained in ME and DSMC in the entire range of temperatures considered here, even though the models are based on different QCT data sets. The NS relaxation times, which again use the MW expression, are significantly higher than the kinetic results. While ME and DSMC results are believed to be more reliable, accurate experimental data may be needed to address these differences.

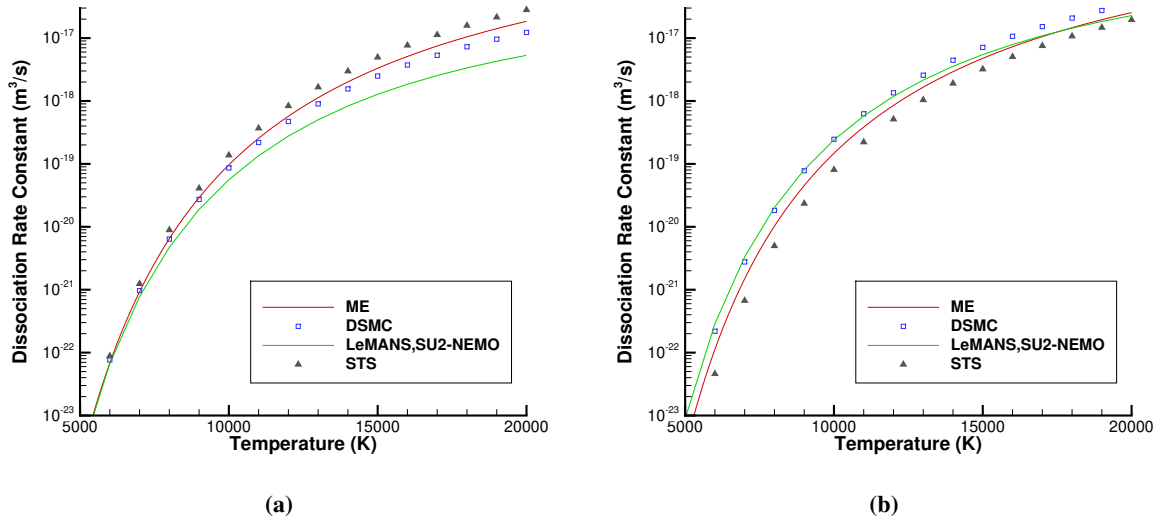


Fig. 5 Dissociation rate constant for N_2 - N_2 (a) and N_2 -N (b) reactions.

Comparison of reaction rate constants used in different codes indicates that differences, and thus uncertainties, are visibly more significant for nitrogen than for oxygen. This is illustrated in Fig. 5 (compare that to Fig. 3 for oxygen). For N_2 - N_2 collisions, Fig. 5a, the difference between the codes does not exceed 20% for $T < 8,000$ K, but quickly increases with temperature, approaching an order of magnitude at $T > 15,000$ K. The NS solvers use the lowest rate constant. The ME rate constant, based on the most recent QCT results, is significantly higher. Clearly, experimental and possibly numerical work may be necessary to resolve the observed differences. There is also some difference, albeit smaller, between the rate constants of N_2 -N dissociation, Fig. 5b. The NS values agree well with the DSMC at lower T and with ME at higher T . The STS values are lower than the other three at all T .

B. Nonequilibrium Rates

Equilibrium reaction rates compared in the previous section provide a zero-order estimate of how fast or slow a particular reaction model, or approach, is expected to relax the gas when compared to the others. They are often the main factor at the quasi-steady-state, where chemical relaxation is slow, and the gas state may be close to equilibrium.

It does not capture, however, the initial stage of the post-shock relaxation, where chemical processes occur under significant thermal nonequilibrium conditions and dissociation reaction rates are strongly impacted by vibrational-dissociation coupling. A better metric in this case is a nonequilibrium rate, which is a function of two temperatures: translation-rotational and vibrational. The ratio of this nonequilibrium rate to the corresponding single-temperature rate, $k(T, T_{vib})/k(T)$, reflects to some degree the vibrational favoring expected for a particular model. The values of this ratio obtained by different solvers at $T = 10,000$ K and varying T_{vib} are shown in Fig. 6 for oxygen. All dissociation reactions are threshold processes, and the general trend of decreasing the ratio is expected for any dissociation model, even a model that does not have any vibrational favoring. This is illustrated by the dashed lines, which show the rate constant ratio for the TCE model of DSMC. There is no vibrational favoring in TCE, and the nonequilibrium rate still decreases from its equilibrium value at 10,000 K by approximately a factor of 3 at $T_{vib} = 4,000$ K. The decrease is slightly more significant for molecule-molecule collisions due to the implementation of the TCE model, where the vibrational energy of the non-dissociating molecule contributes to the reaction cross-section.

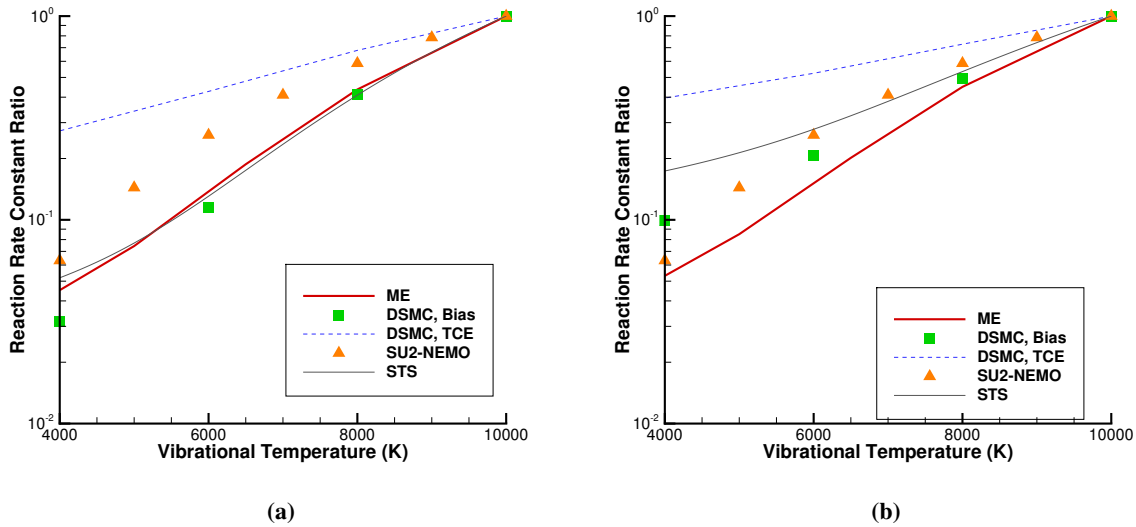


Fig. 6 Nonequilibrium reaction rate constant for O_2-O_2 (a) and O_2-O (b) dissociation.

In the numerical approaches considered here, for which baseline models all take into consideration vibration-dissociation coupling, the dependence of the nonequilibrium reaction rate on the vibrational temperature is much stronger than in TCE. The calculations show that for O_2-O_2 collisions, the Park two-temperature reaction model used in LeMANS and SU2-NEMO has the weakest vibrational favoring. The results for the other three solvers are fairly close. For O_2-O dissociation, there are some differences between the approaches. The dependence on T_{vib} is the weakest in STS and the strongest in ME. Notice that for all three state-specific approaches (ME, STS, and DSMC) the dependence of the rate ratio on T_{vib} is nearly linear, while in Park's model, the trend is different, and the values decrease more

significantly at lower temperatures. While it is tempting to assume that state-specific approaches, and in particular, QCT-based ME, provide better accuracy in that regard, experimental validation would be necessary to prove this point. Comparison of nonequilibrium reaction rates was also conducted for nitrogen; results similar to oxygen were obtained and thus not shown here.

C. 0D and 1D Relaxation with QCT- and Data-Based Rates

The primary way to evaluate the validity of a numerical approach is to compare the results of numerical modeling with available experimental data. At this time, there is little experimental data that would offer such an opportunity for high-temperature nonequilibrium relaxation of neutral oxygen or nitrogen behind a strong shock wave. For nitrogen, the authors are not aware of such data; for oxygen, there are incident shock wave experiments [6] and reflected shock wave experiments [14] for oxygen-argon mixtures. For incident shock waves, in particular, it was found [91, 92] that modern absorption diagnostics [6] may not offer sufficient resolution to distinguish between low- and high-fidelity models for shock velocities below 4.5 km/s. For reflected shock waves, accurate capturing of time-resolved interactions of an incident shock with the wall is necessary [93], thus requiring a modification in the numerical algorithm such as that proposed for the DSMC method [93]. It is therefore beyond the scope of this work to model a reflected shock with different numerical approaches, although it may be a topic of a separate study.

For the post-shock adiabatic relaxation problem considered here, the availability of well-resolved vibrational relaxation times and reaction rates for high-temperature oxygen [14] provide an opportunity to evaluate how these rates impact numerical results when compared to the case based on theoretical (QCT) rates. In this work, we used the DSMC code as a testbed to implement best-available experimental and theoretical rates for VT relaxation and chemical reactions in oxygen. Both the LB model for VT relaxation and TCE model for chemical reactions provide a simple way to directly incorporate temperature-dependent relaxation times and rate constants into DSMC, and thus are applied here for this purpose, with the most recent rate information available. The analytical recommendations based on the corresponding experimental data of Refs. [12, 14] and Ref. [6] are used for molecule-molecule and molecule-atom collisions, respectively. For the theoretical rates, QCT-based information from the current ME modeling is used. Note that in the comparison below, we disregard the excitation of the electronic degrees of freedom. The reasons for this are (i) it is not taken into account in the corresponding QCT calculations, and (ii) electronic excitation is believed to be low during the initial stage of the relaxation behind a shock wave, either incident or reflected, where the relaxations times and reaction rates were evaluated.

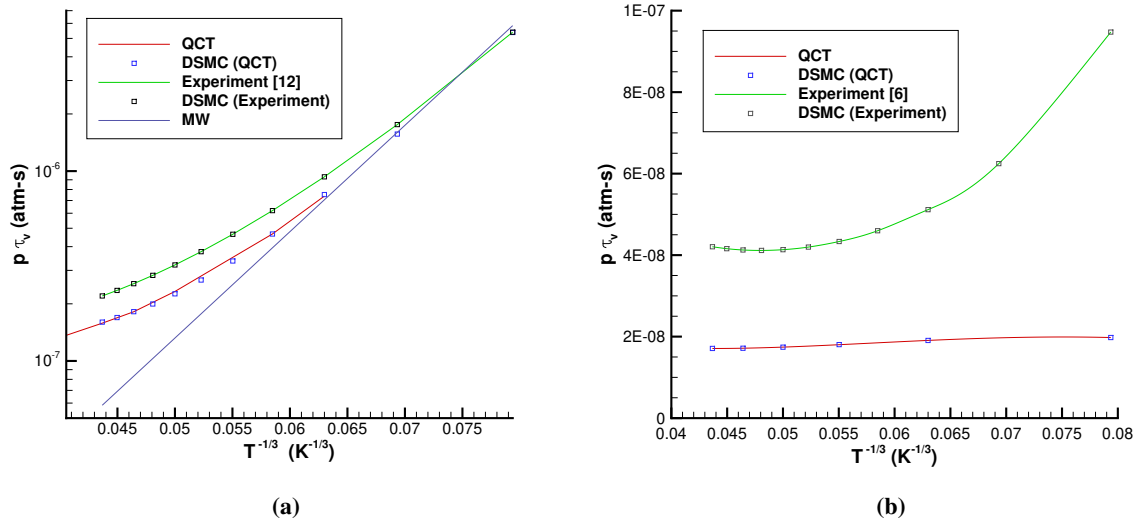


Fig. 7 QCT and experimental data-based vibrational relaxation time for O_2-O_2 (a) and O_2-O (b) collisions.

First, let us compare the experimental and theoretical rates that were applied in DSMC. The values of τ_v for molecule-molecule and molecule-atom collisions are shown in Fig. 7. The measured τ_v for O_2-O_2 is approximately 25% higher at low temperatures, and that difference increases with temperature to almost 50%. Still, the agreement is believed to be reasonable, taking into consideration experimental and theoretical uncertainties (the experimental error bars are estimated to be approximately 25% at low T , and about 50% at high T ; the theoretical error bars are not known but believed to be at least as big as the experimental ones due to a number of model related and numerical uncertainties). Note also that the slopes of both the experimental and theoretical curves noticeably differ from that of MW, even at low T . The DSMC relaxation times which approximate the experiment and theory are also shown; the LB model is used for both molecule-molecule and molecule-atom collisions, as it provides a nearly perfect match for them. The τ_v values for O_2-O collisions show a significant difference between the theory and experiment, which increases from a factor of 2.5 at high T to a factor of almost 5 at low T . This is not surprising, as the experimental recommendations, as indicated in Ref. [6], have unknown error bars, which may be as high as an order of magnitude at low T . Better quality data may therefore be needed for this interaction.

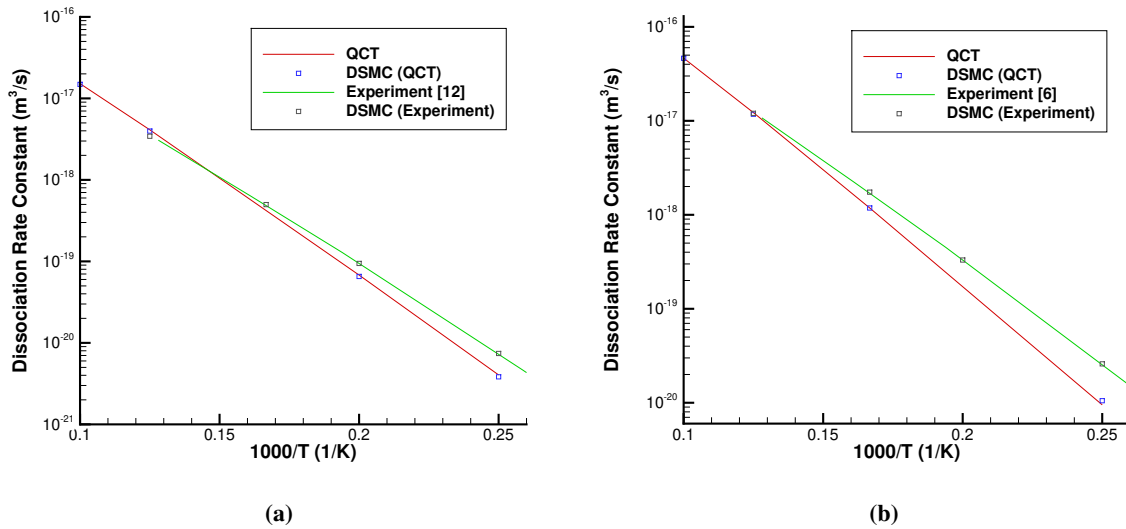


Fig. 8 QCT and experimental data-based dissociation rate constant for O_2-O_2 (a) and O_2-O (b) reactions.

Experimental and theoretical oxygen dissociation rates used in this section are presented in Fig. 8. For both reactions, the QCT slope is sharper than the corresponding slope recommended by the experimentalists; in both cases, they cross at approximately 8,000 K. The general agreement is good for the O_2-O_2 dissociation, where the QCT curve is mostly within the experimental uncertainty of approximately 30%. The agreement is worse for O_2-O , where the difference reaches a factor of three, although experimental error bars in this case are not known to the authors. It should be noted that differences of this magnitude can be expected, even between high-fidelity theoretical predictions and quality measurements. For the former, there are uncertainties in the determination of the corresponding potential energy surfaces, the fitting of these surfaces to find inelastic and reaction cross-sections, and the adaptation of these cross-sections to a particular flow model. For the latter, there are a number of instrument, facility, and data interpretation uncertainties.

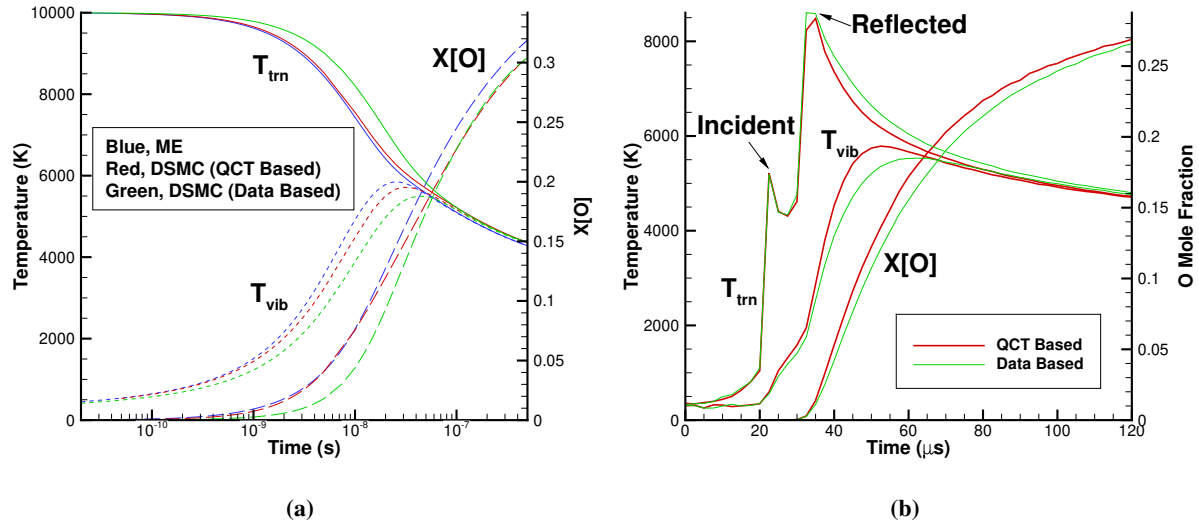


Fig. 9 QCT and experimental data-based computations of heat bath (a) and reflected shock (b). Heat bath: ME and DSMC approaches; reflected shock: DSMC approach.

Results of the DSMC modeling of an adiabatic thermal bath of oxygen using the theoretical and experimental rates are summarized in Fig. 9a. ME results that rely on the same QCT rates are also shown. Comparing DSMC and ME, one can see that there are a few relatively small, but visible differences: the ME vibrational temperature peaks approximately 10% earlier, the peak is approximately 3% higher, and the atomic oxygen mole fraction rises slightly faster in ME. Those differences are primarily attributed to inherent differences in the energy dependence of VT excitation and dissociation cross-sections: not only is the energy structure different, but also the exact energy dependence of these processes cannot be precisely matched. Still, the agreement between DSMC and ME is reasonably good. Comparison of DSMC results obtained with experimental and theoretical rates shows that there is visible effect approximately in the first 10 ns. The chemical relaxation is delayed by approximately a factor of two when the data-based rates are used (notice the logarithmic scale on the X-axis). Because of the lower dissociation rate, which may be expected from Fig. 8a, the gas translation-rotational temperature is higher. The vibrational temperature is somewhat lower, which may also be expected from Fig. 7. At longer times, when the gas is close to thermal equilibrium, the impact of the rates is minimal.

A factor of two delay in chemical relaxation may well be within the detection limits of shock tube-based measurements; therefore, the DSMC modeling was conducted in a numerical setting [93] which reproduces the experimental environment and conditions of recent measurements [12]. In this case, transient one-dimensional reflected shock simulations are performed in a pure O₂ gas, which is initially stagnant at a pressure of 40 Pa and a temperature of 296 K, and then exposed to an incident shock moving at a velocity of 2,800 m/s (this is close to the maximum shock intensity achieved in Ref. [12]). To approximate the experiment, the modeled transient gas properties are recorded in a sampling cell centered

at a distance of 5 mm from the wall, so that the effect of the gas-surface interaction is negligible. The gas temperatures and the atomic mole fraction are shown in Fig. 9b, computed for the data and theory-based rates. The temporal profile of the translational temperature shows both the incident and the reflected shocks passing through the sampling cell at approximately 22 and 35 μs , respectively. The vibrational relaxation starts immediately after the passage of the incident shock. The vibrational temperature for the data-based rates is slightly lower due to lower VT relaxation rates (see Fig. 7). The difference, however, is mostly minor and reaches 500 K only near the peak. The differences between the atomic mole fractions are also small, and likely below the detection limit of even a highly accurate measurement. This may be an indication that if the state-of-the-art theoretical and experimental recommendations for molecular oxygen thermal and chemical rates for the range of temperatures 5,000-10,000 K are highly accurate, then further refinements in theoretical and experimental resolution may not provide significant benefit, at least from the modeling perspective.

D. Oxygen Heat Bath: Comparison of Different Approaches

The good agreement between the DSMC results obtained with the most recent data and theory-based rates is certainly an encouraging sign, but there always exists a possibility of further corrections or improvements, experimental and/or computational, in the future. Moreover, many numerical solvers are still using thermodynamic and chemical datasets that rely on less recent, but nonetheless well-respected, sources. In order to assess possible implications of using such sources, the calculations presented here were performed using the “baseline” models and parameters for all the solvers (with one exception discussed below). The temperature relaxation in the oxygen adiabatic bath is presented in Fig. 10a. There is a near perfect agreement between the NS solutions, which is not surprising, as they use the same thermochemical models and rates. The time to reach the maximum vibrational temperature is approximately 6% shorter in LeMANS than in SU2-NEMO, which is thought to be related to the details of the model implementation. Note that such a code-to-code difference may be expected to be somewhat more significant for a kinetic approach, such as DSMC, where there is a larger number of factors which impact the solution than in a continuum, two-temperature solver.

The vibrational relaxation is faster in NS when compared to all three state-specific solvers, which is attributed to the use of MW with the Park’s correction for O₂-O₂ VT energy transfer in NS (see Fig. 2a). Vibrational relaxation in STS is the slowest, which is partially due to the Morse parameters assumed in the FHO (STS) and FHO-FR (DSMC) models, and also due to the known differences [63] between FHO and FHO-FR. It is also notable that the equilibrium temperature values are close, within less than 5%, for all solvers. The reason for the observed differences in the equilibrium state are equilibrium constants, or backward (recombination) reaction rate constants. In both NS solutions shown here, the Gibbs free energy approach is used to calculate backward reactions. This approach was found to produce results almost indistinguishable (and thus not shown here) from those based on Park’s polynomial expansions of thermodynamic properties [60]. The latter ones are fairly close to the NASA recommendations [42], which were assumed in DSMC. All these polynomial expansions used for thermodynamic properties of real gases take into account the excitation of the

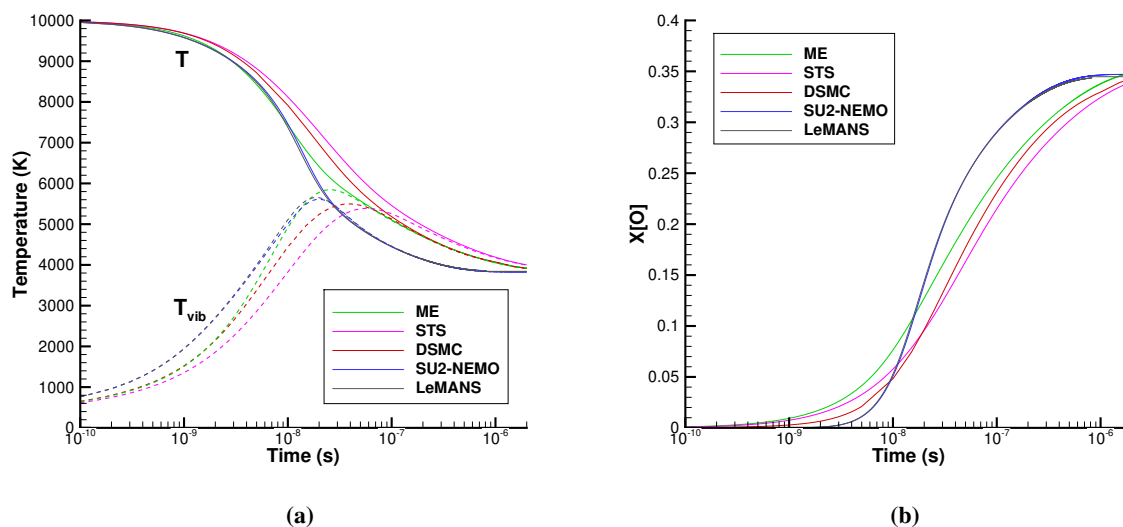


Fig. 10 Gas temperatures (a) and oxygen atom mole fractions (b) obtained by different approaches.

electronic degrees of freedom (EDF). The ME model derived backward rate coefficients by directly computing partition functions of the products and reactants. Because the underlying QCT simulations involve PESs that correlate only with the ground electronic state, the degeneracy of only the lowest-lying electronic states of products and reactants are taken into account in the detailed balance in the ME approach. Similarly, EDF's are not accounted for in STS, where the reverse reaction rates are obtained from the translational, rotational, and vibrational partition functions. Similar to the gas temperatures, the difference in the equilibrium state has small impact on the atomic oxygen mole fraction profiles, shown in Fig. 10b.

The electronic excitation is not taken into account in the baseline DSMC model, even though the reverse reaction rates are calculated with equilibrium constants that account for electronic excitation. Note that a separate DSMC calculation was conducted that did take into consideration the excitation of EDF's of both O_2 and O , where the discrete-level model of Ref. [94] was applied. The results obtained by this model are presented in Fig. 11a, where they are compared to the baseline. Generally, the translational and vibrational temperatures slightly decrease when electronic excitation is considered, but the effect is small. The largest difference, of approximately 60 K, is observed near the peak vibrational temperature. The Bias model of dissociation used here did not take into account the influence of electronic excitation on chemical reactions, and the atomic fraction for the EDF-included case lags that of the baseline. A more realistic model, which incorporates EDF's into the reaction cross-sections, would likely have an opposite effect on $X[O]$, and thus reduce the deviation from the baseline. Small effect of the electronic excitation may be explained by relatively low number of the corresponding electronic degrees of freedom, as illustrated in Fig. 11b. Due to slow electronic excitation, electronic temperature does not rise above approximately 4500 K, so that the number of the electronic degrees of freedom does not

exceed 0.5, as compared to the translational-rotational-vibrational degrees of freedom of almost 7.

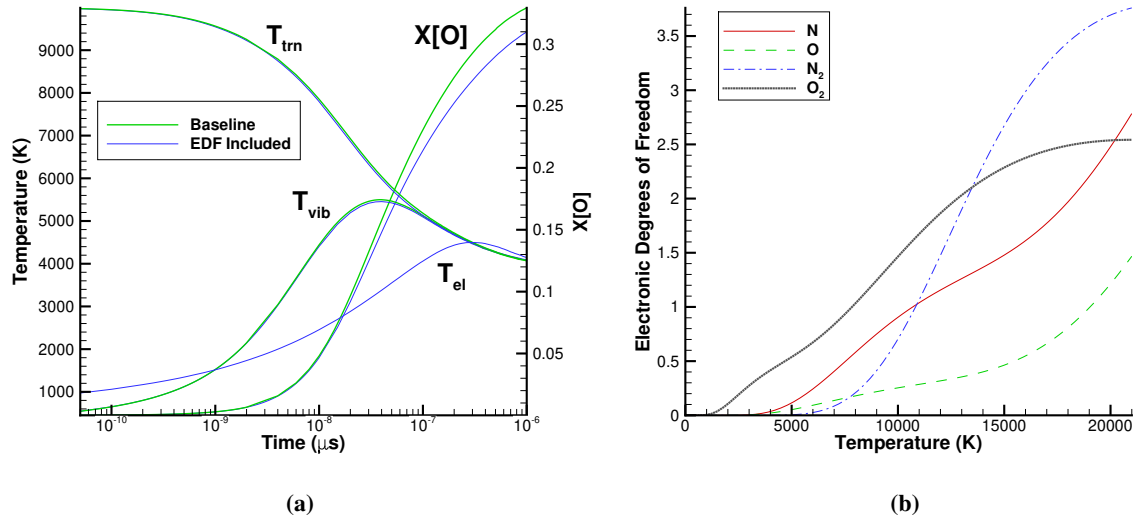


Fig. 11 Electronic degrees of freedom: oxygen heat bath relaxation computed by DSMC computation without and with the excitation of the electronic degrees of freedom (a), and the DSMC-based number of the electronic DOF of atomic and molecular species (b).

E. Oxygen Heat Bath: Impact of the Model

The differences between the results obtained with the five numerical solvers discussed in the previous section to a large extent may be attributed to the vibrational relaxation and chemical reaction rates. As discussed earlier, each solver includes real gas effect models that either directly rely on, or are calibrated with, single-temperature rates (data or theory based) which the authors of the solver believe to be the best available. Such rates, however, may need to be updated as new experimental or computational results appear in the literature. An example of such an update is shown below. Earlier STS calculations, such as [48, 95], modeled O_2 - O_2 dissociation on QCT calculations [96] that were current at the time. Those QCT results used an earlier potential energy surface [97]. The publication of a potential energy surface [44] that is believed to be more accurate prompted an update in the QCT calculations, with the new reaction rate constants presented earlier in this work. The updated rates differ significantly from those published earlier [96], especially at low and moderate temperatures, which motivated the corresponding update in the baseline STS model parameters for O_2 - O_2 : the rate coefficients used in the present STS implementation, although based on the modified Marrone–Treanor model [50], are in good agreement with those obtained using the PES from [44].

Comparison of gas temperatures and atomic mole fractions for the STS solver using the dissociation model with parameters that provide a good approximation for the old [96] and the current rates is presented in Fig. 12a. There is a significant difference between the results, which indicates that the accuracy of a high-fidelity model is defined by

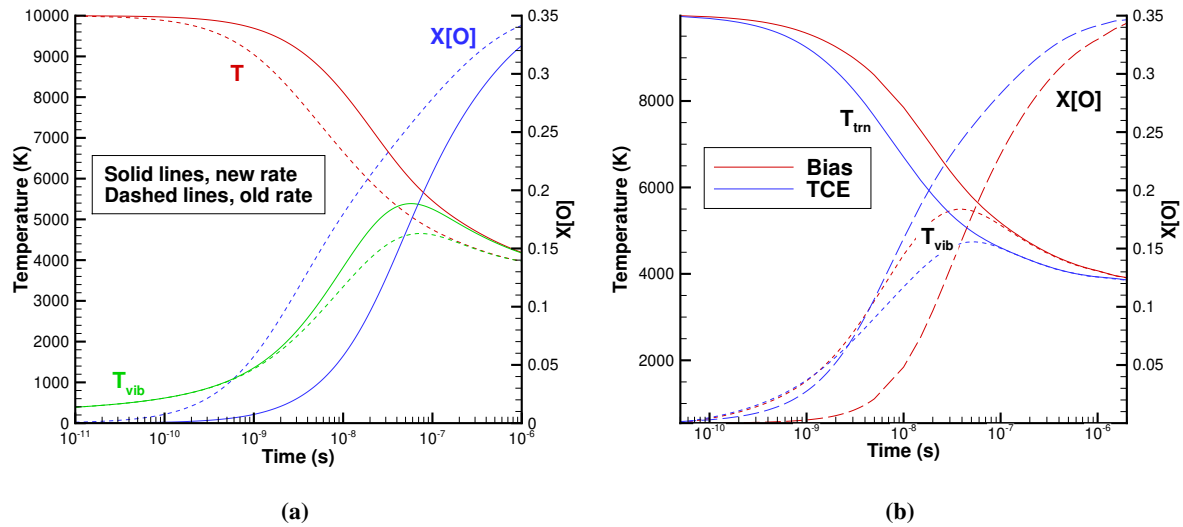


Fig. 12 Impact of O_2-O_2 dissociation reaction rate in STS (a), and baseline vs conventional energy transfer and reaction models in DSMC (b).

the accuracy of the underlying kinetic data rooted in the fidelity of the quantum-mechanical models used to solve the Schrödinger equation describing the motion of electrons and nuclei.

As expected, the most pronounced difference is in the oxygen mole fractions, where the updated rate causes an order of magnitude slower dissociation rate. This, in turn, results in significantly higher translational temperatures and, to a lesser degree, vibrational temperatures. Even though the new dissociation rate constant may benefit from further validation, this example shows the importance of relying on the most recent single-temperature reaction rates.

While the consideration of the most accurate single-temperature rate constants is important, it is not sufficient for numerical simulation of dissociating oxygen to be reliable. Yet another factor is related to capturing vibration-dissociation coupling. A model that accurately reproduces single-temperature rate constants may not perform well if it does not offer a reasonable degree of vibrational favoring specific for each reaction. Such a model may fail in providing accurate time relaxation under conditions of significantly lower vibrational temperature, typical of post-shock relaxation. An example of such failure is shown in Fig. 12b. In this figure, two DSMC models are compared: the baseline Bias model which takes into account vibrational favoring and is calibrated with QCT data for both oxygen dissociation reactions, and the TCE model that does not have any vibrational favoring. The rate constants are nearly identical in these models, but the relaxation of the macro parameters is very different. The lack of vibration-dissociation coupling in TCE results in much faster relaxation. The faster relaxation, in turn, is the reason for a lower value of maximum T_{vib} in the TCE model.

In the two-temperature solvers, two dissociation models are used: a preferential model (the baseline) and a non-preferential model. The difference between these two is not in the vibrational favoring of the reaction cross-section

as was in the Bias and TCE models of DSMC, but rather in the vibrational energy loss due to dissociation. In this comparison case, the impact of the model is much smaller, as illustrated in Fig. 13, and manifested primarily in a slightly lower maximum vibrational temperature for the preferential model. The TCE-LB model of DSMC is also shown for comparison, with both VT transfer and dissociation rates set to match those of SU2-NEMO.

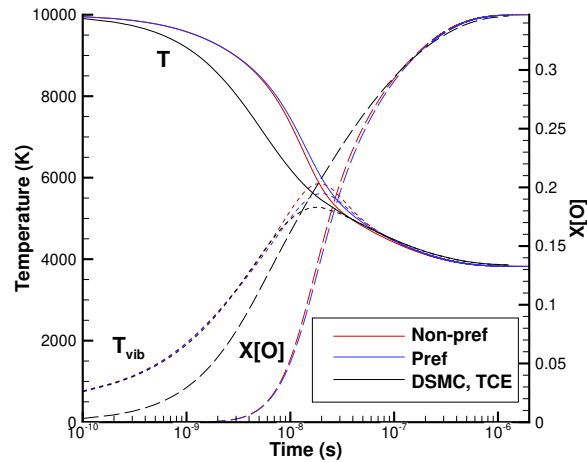


Fig. 13 Impact of the reaction model in SU2-NEMO.

F. Thermal and Chemical Nonequilibrium Effects

The effects of thermal nonequilibrium, discussed in the previous section, are manifested at two levels: macroscopic and microscopic. At the macroscopic level, there is a difference between the translational, rotational, and vibrational temperatures (albeit only the translation-vibration nonequilibrium is included in all the approaches used here except DSMC). At the microscopic level, there are nonequilibrium energy distribution functions. The most important of which pertains to the vibrational mode since the preferential depletion of higher vibrational levels results in the suppression of the dissociation rate. The impact of this vibrational nonequilibrium is therefore examined below in more detail.

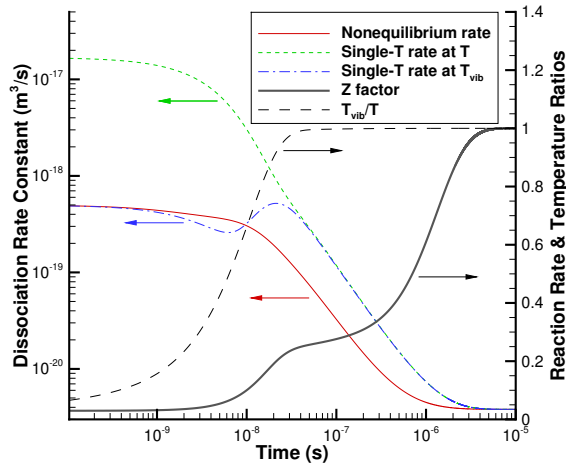


Fig. 14 O_2 - O_2 dissociation rate constants and ratios obtained by the ME model. The arrows show the Y axis for the corresponding line.

Let us first compare the nonequilibrium and the corresponding single-temperature rates for the oxygen adiabatic bath problem. These rates, obtained by the ME approach, are shown in Fig. 14. In this plot, “Nonequilibrium” stands for the actual O_2 - O_2 reaction rate as it was recorded in the simulation. “Equilibrium at T ” and “Equilibrium at T_{vib} ” are the reaction rates calculated with the single temperature expressions (see Fig. 3a) that use the instantaneous values of T and T_{vib} , respectively. At the early stage of the relaxation, approximately over the first nanosecond, the reaction rate is governed by the very low vibrational temperature, and the actual rate is close to the single-temperature rate at the local T_{vib} , $k_{eq}(T_{vib})$. Note that the degree of dissociation is negligible at this point (see Fig.10b). As time progresses, $k_{eq}(T_{vib})$ starts to diverge from the actual rate k , moving first below and then above k . At a time when the gas translation-rotational and vibrational temperatures become close (see the temperature ratio T_{vib}/T , also shown in the figure), which occurs at approximately 30 ns, the single-temperature rates at T and T_{vib} merge. However, the nonequilibrium rate at this time is much lower. This is clearly due to the dissociation-driven depletion of higher vibrational levels, which has a disproportionately high effect on the dissociation rate, but very little impact on vibrational temperature. Such behavior has an interesting effect on the ratio of the “Nonequilibrium” rate k to the “Equilibrium at T ” rate $k_{eq}(T)$, which is called the “Z factor” hereafter, and also plotted in Fig. 14. The Z factor starts to rise from nearly zero after the first nanosecond, to 0.25, when it reaches a plateau (the degree of dissociation is still only about 0.3 at this time, see Fig.10b). The plateau spans from 30 ns to 300 ns. During this time, the degree of dissociation increases from 0.3 to almost 0.9. The plateau has all features of the quasi-steady-state [88], with depleted high vibrational levels, the vibrational temperature approaching the translational temperature, and relatively slow dissociation, at least when compared to the vibrational relaxation.

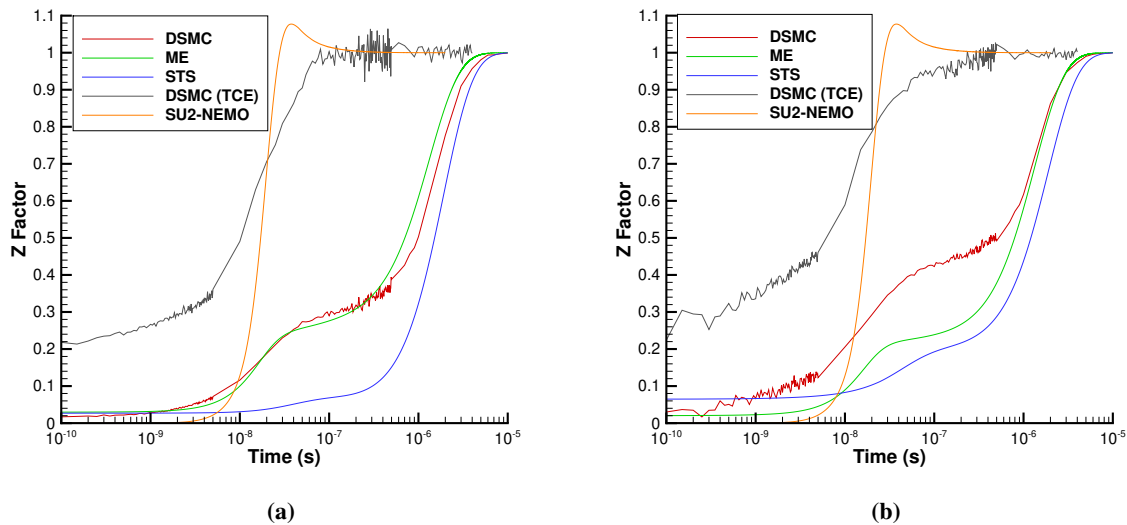


Fig. 15 Reaction rate ratio for O_2-O_2 (a) and O_2-O (b) reactions.

The authors believe that the existence of such a plateau is a physical model related, and not numerical, effect, but it may only be observed when a state-specific approach is used which takes into account vibration-dissociation coupling. To illustrate this, the Z factor was computed using each approach. For DSMC, both the VDF Bias model and the non-VDF TCE model of dissociation are used. The results are summarized in Fig. 15, where the Z factor is plotted for the two reactions. For the O_2-O_2 reaction, the ME and baseline DSMC profiles are nearly the same: both have a plateau, and their formation times and heights are very similar. When the TCE model is used in DSMC, there is no plateau. Note also that for the TCE model, the Z factor starts from a much higher value than ME and DSMC-Bias. For the former, the initial value of the Z factor is about 0.2, while for the latter, it is nearly an order of magnitude less. This is because even for molecules at their ground vibrational state, the dissociation probability in TCE is still quite significant, provided the rotational and relative translational energies are high enough. For the state-specific STS model, the Z factor also starts from a low value of 0.03, very close to that of ME. There is also a plateau observed for STS, although less pronounced than for ME and DSMC, and at a significantly later time. Generally, there are several factors that impact the height and the flatness of the plateau, the most important ones being the model of the state-to-state vibration-translation energy transfer and the degree of the vibration-dissociation favoring. In STS, the population of the upper vibrational levels is significantly delayed, as will be shown below, and the vibration-dissociation favoring is somewhat weaker in STS than in the other two state-specific approaches. These effects result in the delay in the formation of the plateau in STS (also compare that to slower vibrational relaxation illustrated in Fig. 10a). The NS solutions (SU2-NEMO and LeMANS results are close, so only one of them is shown here) do not have a plateau, but both show a small but visible peak near the point where the vibrational and translation-rotational temperatures equilibrate. This is an effect that is

believed to be related to Park's $T_c = \sqrt{T \cdot T_{vib}}$ assumption rather than to a particular physical mechanism. Note also that the Z factor is initially zero in the NS model, which is another numerical effect related to the above assumption. Notice also that Z factor reaches the unity much earlier in the Navier-Stokes solutions and DSMC-TCE than in all three state-specific approaches. This is because the former depends on the time when the vibrational temperature approaches the translation-rotational temperature, while in the latter, there is strong dependence on the populations of the upper vibrational levels. These levels, with populations orders of magnitude lower than that of the upper levels, as will be discussed below, contribute little to the vibrational temperature (or average energy), but very important for dissociation reactions.

General trends observed for the O_2-O_2 dissociation holds for the O_2-O reaction as well, as shown in Fig. 15b. In this case, however, there is a noticeable difference in the height (but not the location) of the plateau observed in the ME and DSMC approaches. Generally, for the same model, the height of the plateau is expected to depend primarily on the degree of vibrational favoring of that model; the higher the favoring, the lower the plateau. In DSMC, for example, the exponent ϕ (a parameter that controls the degree of the vibrational favoring) is 4 for molecule-molecule, and 2 for a molecule-atom reactions. Thus, the height of the plateau is approximately 0.3 and 0.45, respectively. For O_2-O dissociation, ME appears to exhibit a higher degree of vibrational favoring than DSMC (see also Fig. 6b), thus, the plateau is lower. There is also some difference between STS, ME, and DSMC when the vibrational excitation is very low, which also points to different degrees of vibrational favoring. This is not surprising, as larger uncertainties are expected for this reaction than for the much better studied O_2-O_2 interaction.

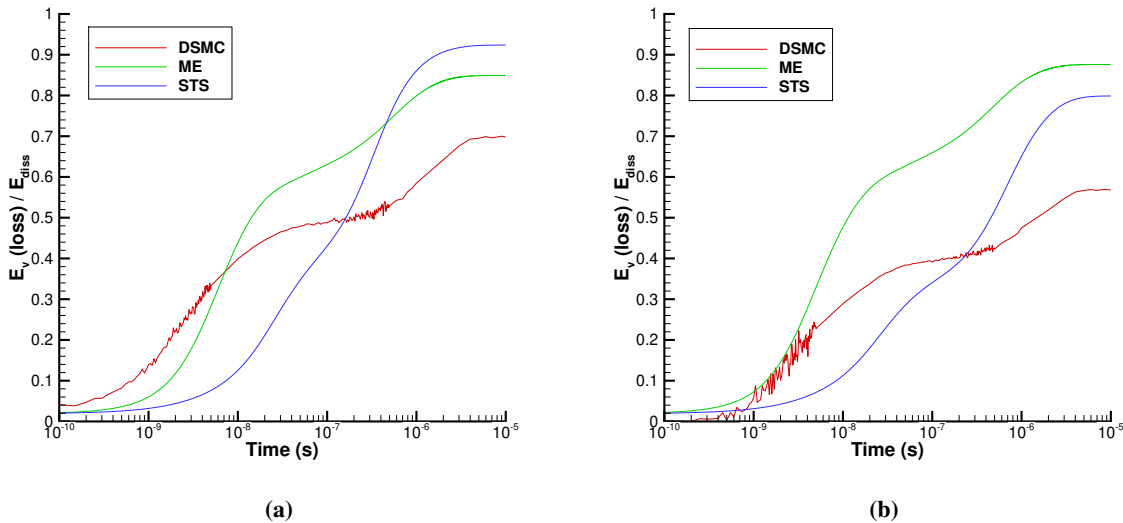


Fig. 16 Average vibrational energy loss in O_2-O_2 (a) and O_2-O (b) dissociation.

Let us now examine the average vibrational energy loss in dissociation — one of the gas properties related to the

vibration-dissociation coupling. Being also a direct product of such a coupling, it may be regarded as a microscopic property when calculated per dissociation event; in this case, it is equivalent to the average vibrational energy of dissociating molecules. This average vibrational energy loss per dissociation event, normalized by the reaction threshold, and obtained by the state-specific approaches, is shown in Fig. 16 for the O_2-O_2 and O_2-O reactions. In all three approaches, the initial energy loss is close to zero due to the very low population of upper vibrational levels at that time. Then, it increases quickly due to the VT relaxation. In the STS approach, the increase is steep, and the normalized energy loss quickly reaches its equilibrium value of about 0.9 for the molecule-molecule reaction, and a somewhat lower 0.8 for the molecule-atom reaction. The slope changes somewhat at a time that corresponds to a weak plateau in Z factor shown earlier in Fig. 15. That behavior differs qualitatively from DSMC, where there is a well defined plateau, also formed accordingly to the Z factor. Similar to the Z factor, the energy loss plateau is attributed to the depleted high vibrational levels at the quasi-steady-state discussed earlier. In ME, the plateau is significantly less pronounced than in DSMC, and its values are higher. Same as in Z factors, the main reason for differences in STS vs DSMC and ME is the vibration-translation model and the degree of vibrational favoring assumed in these approaches (in ME, as well as in DSMC, it is higher than in STS). For a majority of the relaxation, the energy loss is generally higher in ME than in DSMC, especially for the O_2-O reaction. ME is the only approach which indicates that the vibrational energy loss may be higher in the molecule-atom than in the molecule-molecule reaction. Note that in ME, the obtained degree of vibrational favoring is similar for O_2-O_2 and O_2-O , while for DSMC and STS, it is assumed more significant for O_2-O_2 (cf. Fig. 6a and 6b).

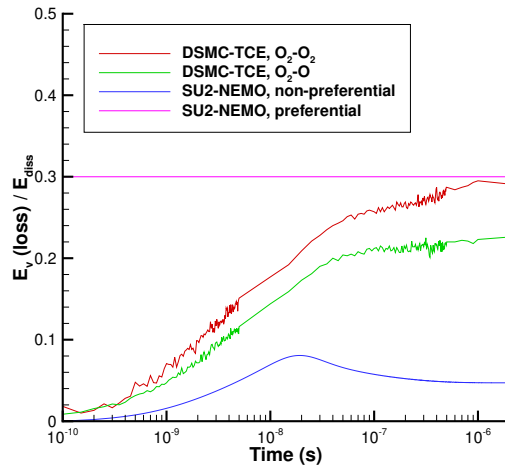


Fig. 17 Average vibrational energy loss in oxygen dissociation when colliding with O_2 and O : DSMC method based of the TCE model and the continuum approach for two models of dissociation (the models do not differentiate between the collision partners).

While the baseline, vibrationally coupled DSMC model indicates that there may be a plateau when the gas reaches a

quasi-steady-state, the conventional, non-VDF model of DSMC cannot be expected to produce such a plateau. This is illustrated in Fig. 17, where the results obtained with the TCE model are presented for the two reactions. Similar to the Bias model, TCE predicts a higher vibrational energy loss in molecule-molecule collisions than molecule-atom collisions. The average vibrational energy loss was also computed with the NS solvers; SU2-NEMO results are presented here for the preferential and non-preferential dissociation models (LeMANS results are very similar and thus not shown). In the preferential dissociation model, the dissociation from both O_2 - O_2 and O_2 - O collisions is assumed to remove a fixed 30% of the dissociation energy, thus there is a flat line at $0.3E_D$ for that model. Note that the equilibrium values for the TCE model are fairly close to the assumed NS value, but for the state-specific approaches they are significantly higher (Fig. 16). For the non-preferential model, the average vibrational energy loss is much lower and does not exceed $0.1E_D$ even at its peak, which occurs at approximately 20 ns (compare this to the maximum in Z factor at approximately 30 ns, Fig. 15).

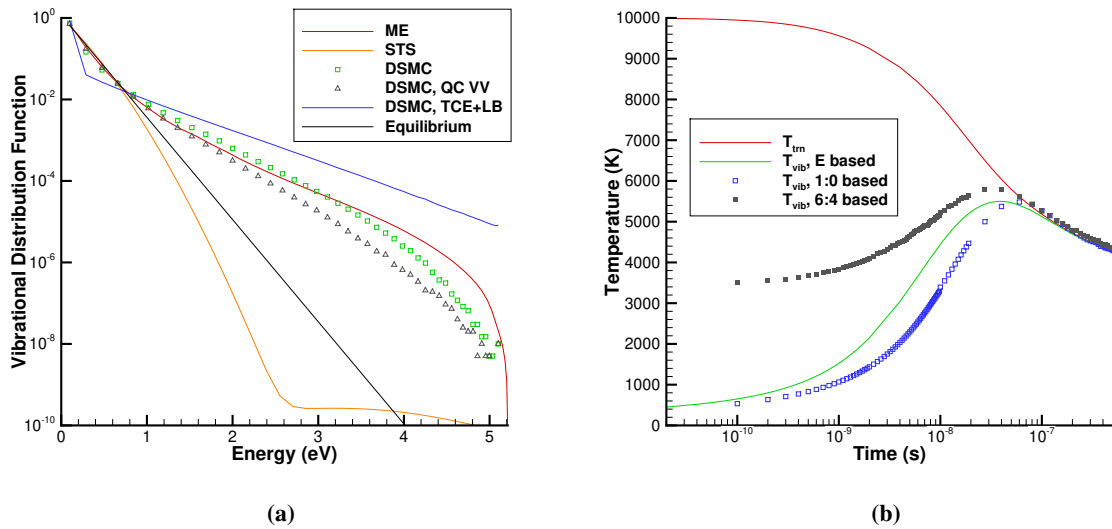


Fig. 18 Vibrational distribution function at 2000 K computed with different numerical approaches and models of DSMC (a) and DSMC vibrational temperature based on average energy and two population ratios (b).

When a vibrationally coupled model of dissociation, used in a state-specific approach, is applied to simulate chemically and thermally nonequilibrium flow, the results always depend on the vibrational distribution function. This is valid for the quasi-steady-state, but is expected to be especially noticeable at the earlier stages of relaxation, where the vibrational temperature is lower than the translational temperature. To assess this aspect of the numerical approach and model, instantaneous vibrational populations of O_2 were sampled at a point in time when the vibrational temperature reached 2,000 K. The results are presented in Fig. 18a. The baseline ME and STS models are shown, along with three DSMC vibrational relaxation and dissociation models. The first, labelled “DSMC”, is the baseline. In the second model,

labelled “DSMC, QCT VV”, the empirical near-resonant model of vibration-vibration (VV) transitions used in the baseline is replaced by the quasiclassical model [82]. It is possible that this model is somewhat more accurate than the baseline, and it certainly promotes more significant VV transfer. The model is only applicable to collisions of the same molecular species, and thus is not used as the baseline. In the third model, “DSMC, TCE+LB”, TCE is used for dissociation, and LB replaces FHO-FR to simulate VT energy transfer, with no VV included.

Comparing the baseline DSMC VDF with that of ME, one can see that there is a good agreement, both qualitative and quantitative, between the two. The computed slope for a few lower levels approaches that of the corresponding equilibrium ($T_{vib} = 2,000$ K) VDF, but then becomes much less steep. For very high levels, with energy approaching the dissociation threshold of 5.1 eV, the slope becomes steeper again. This is especially noticeable in ME and related to the energy depletion in vibrationally-favored dissociation. When the QC VV model replaces the baseline in DSMC, the vibrational population slope becomes somewhat steeper, and the impact of dissociation is less pronounced. This VV effect, however, is relatively minor (and almost non-existent in macroscopic properties, thus not shown here). The effect of replacing FHO-FR with LB is much more significant. In this case, there is essentially a two-temperature shape of the VDF, with the first-to-ground level population ratio approaching that of the initial vibrational temperature, and the rest approaching the translational temperature. The most noticeable aspect from Fig. 18a is that the VDF for the STS model is qualitatively different from those of DSMC and ME. There are several factors that contribute to the shape of the VDF. For molecules that reside at vibrational states below approximately 2.5 eV, the primary contributor is dissociation, which effectively depletes these states (with some preference to higher states, thus the changing slope of the left branch). For molecules with higher vibrational energies (the right branch), the shape is strongly affected by the recombination. Also, there is some impact of VV, which preferentially populates the middle part of the spectrum, and depopulates the upper levels (above 3.7 eV).

The above example shows that even though the shape of the VDF differs in each approach, they all predict the vibrational population to be strongly non-Boltzmann. This immediately raises the question of how the vibrational temperature should be defined. Probably the most obvious answer is to define it based on the average vibrational energy, combined with the Boltzmann expression for vibrational populations. The average energy is represented as a sum over all vibrational levels assumed to be populated as if there was equilibrium with some effective temperature, and the temperature is then found numerically (or analytically for the simple harmonic oscillator). Such an approach may arguably be considered preferable when one needs to compare state-specific results to continuum, temperature-based solutions, and thus is used in this work. However, such an approach will result in a vibrational temperature significantly different from that calculated using the first-to-ground level population ratio, often applied in the past. Moreover, in modern experiments [6, 12], populations of higher vibrational levels, such as 4 and 6, are detected in oxygen, and the vibrational temperature is inferred from that population ratio under the Boltzmann assumption. To illustrate the implications of the choice of the approach to T_{vib} calculation, the DSMC vibrational populations were taken to calculate

T_{vib} with the average-energy and population-ratio based methods. The results are shown in Fig. 18b. Here, the baseline DSMC model is used (labeled "DSMC" in Fig. 18a). The population-based vibrational temperatures differ significantly from the average-energy-based temperature. The difference is especially large for the 6:4 ratio (this ratio was used in recent measurements [12, 14]). Both DSMC and ME calculations indicate that the vibrational temperature based on the 3:0 level population ratio provides the best match to the average-energy-based T_{vib} , although Fig. 18a indicates that this result could be approach- or even model-specific. The figure shows the importance of using the correct temperature definition when comparing to experimental data.

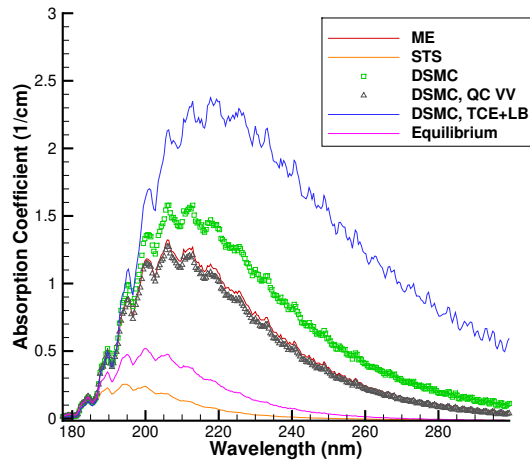


Fig. 19 UV absorption coefficient calculated from the populations of vibrational levels 4 and 6: the impact of the numerical approach.

Not only are vibrational populations important when analyzing and validating the computed vibrational temperatures, but also when numerical models are validated through comparisons with UV absorption measurements. One possible way to compare to such measurements is to compute vibrational populations and then, for specific vibrational levels used in a benchmark experiment, infer vibrational temperatures and use them in a temperature-based spectral code, such as Neqair or Specair [98, 99]. The computed vibrational populations will thus have a big impact on the calculated spectra. An illustration of such an impact is given in Fig. 19, where the populations of vibrational levels 4 and 6, shown in Fig. 18a, and converted to temperature under the equilibrium assumption, are used in the Neqair v15.0 code to obtain UV absorption spectra. The corresponding population-based vibrational temperatures are used in Neqair along with the translational and rotational temperatures recorded at that time. The notations correspond to those in Fig. 18a. Only two of the results agree well, ME and DSMC with QC VV (although the baseline DSMC is also relatively close to those two), all others differ noticeably. Four of the five computed spectra are higher than the corresponding vibrationally equilibrium spectra. The difference between the lowest (STS) and the highest (DSMC, TCE LB) absorption coefficient profiles exceeds an order of magnitude. Clearly, such a difference would be measurable, but even good agreement with

data may not fully validate a model (see, for example, noticeable difference between the vibrational populations of ME and DSMC, QC VV, which have very similar absorption spectra). A state-specific spectral code such as Spektr [100] may be needed in this case.

G. Nitrogen Heat Bath: Comparison of Different Approaches

Comparison of single-temperature reaction rates and VT relaxation times, presented earlier, indicated that for nitrogen there is a larger uncertainty and larger differences in the thermal and chemical rates than for oxygen. It is therefore not surprising that there are quite significant differences in thermal relaxation observed for the N_2 adiabatic bath. This is shown in Fig. 20a, where the translation-rotational and vibrational temperatures are shown. Comparing the two Navier-Stokes solvers, one can see that there is a small, but visible difference, with LeMANS relaxation being approximately 10% slower. This code-to-code difference is attributed mostly to implementation details, as the physical models and rates used in the codes are essentially the same. The initial vibrational relaxation in DSMC is much slower than in NS, which is certainly related to the differences in N_2 - N_2 vibrational relaxation times for the FHO-FR model and MW expression with Park's high-temperature correction (see Fig. 4a). The STS relaxation is close to DSMC in the first 10 ns, but then deviates from it due to significantly slower vibrational relaxation in the FHO model used in STS. For the solution of ME, the vibrational temperature relaxes faster than in DSMC, but slower than in NS, while the translational temperature is close to NS, as the dissociation starts earlier in ME. Interestingly, the peak vibrational temperature is approximately the same in all five numerical solutions.

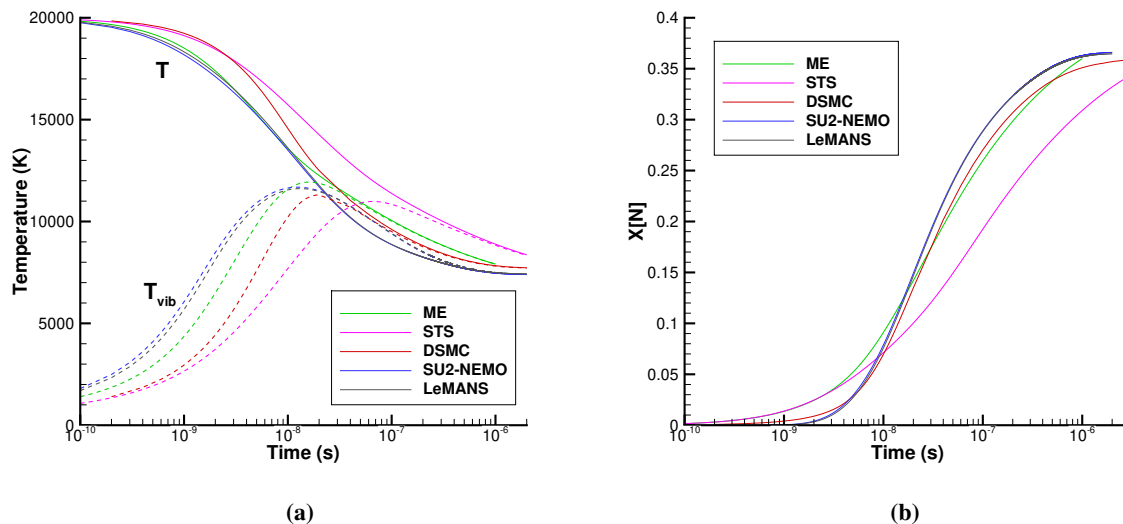


Fig. 20 Gas temperatures (a) and nitrogen atom mole fractions (b) obtained by different approaches.

The differences in the atomic nitrogen mole fractions, obtained by ME, DSMC, and NS (Fig. 20b), are relatively

minor, with the exception of the initial 10 ns, where the ME dissociation proceeds much faster. This may appear somewhat unexpected, keeping in mind noticeable differences between the single-temperature reaction rate constants shown in Fig. 5. Comparing the mole fraction evolution with gas temperature profiles, though, one can see that most of the mole fraction increase occurs when the gas translation-rotational temperatures decrease from 15,000 K to 10,000 K, with the vibrational temperature being on the order of 10,000 K. Dissociation rate constants for this temperature range are approximately a factor of two to three slower in the Navier-Stokes solvers than in DSMC and ME. However, the latter approaches have a higher degree of vibration-dissociation coupling, as illustrated earlier in Fig. 6, which reduces the dissociation rate. This explains similar profiles of the nitrogen mole fraction. The STS solution differs from the other four in the general slope of the mole fraction. The primary reason for this is believed to be the vibrational relaxation, with slowly relaxing higher vibrational levels (see Fig. 18a), which significantly reduces the dissociation rate.

V. Conclusions

Multiple two-temperature CFD, vibrational state-specific, and fully kinetic solvers have been applied to model thermal and chemical processes in high-temperature oxygen and nitrogen adiabatic heat baths. In the baseline analysis, the solvers used their standard vibrational excitation and reaction models and constants. Comparison of single-temperature and nonequilibrium rates show that the largest differences are observed for molecule-atom vibration-translation relaxation and N_2-N_2 dissociation, especially at higher temperatures. High-accuracy shock-tube data, currently nonexistent, may be required to address these differences. For oxygen, state-of-the-art theoretical and experiment-based relaxation rates are relatively close, and differences associated in simulated flow fields using them may well fall below instrumental detection limits for the 5,000K-10,000 K temperature range. Still, further refinements to the O_2-O vibrational relaxation times and dissociation from the experimental and computational communities may prove to be useful. This is especially so if some light may be shed onto the vibrational favoring of dissociation reactions and the details of the relaxation of vibrational populations behind strong shocks, both shown to be important in this work.

Detailed comparison of oxygen relaxation modeled with vibrational state-specific and two-temperature approaches shows that there are very significant, and often qualitative, differences in the time-dependent nonequilibrium reaction rates, as well as their ratios to the corresponding single-temperature rates. For all three state specific solvers, which include master equation-based approaches and the fully kinetic direct simulation Monte Carlo method, there is a well-defined plateau observed at a time when the gas vibrational temperature approaches the translational temperature, and the thermal relaxation proceeds through a quasi-steady-state. Such a plateau is attributed to the depopulation of high vibrational energy levels due to dissociation, as such depopulation has little impact on temperature dominated by lower vibrational levels, but disproportionately high impact on the reaction rates. There is no such plateau observed in the two-temperature solutions, although there is a peak, likely model-related, recorded before the gas comes to equilibrium. There are also qualitative differences observed in the transient profiles of the vibrational energy loss to dissociation. The

two-step increase of that property in the state-specific approaches is not captured in the continuum CFD, where the models show either a flat or a non-monotonous increase. All such differences may have significant implications for any hybrid approach that attempts to couple a continuum and a state-specific or a fully kinetic method.

The computations of oxygen and nitrogen baths show a major impact of the vibration-dissociation coupling on the temporal relaxation of gas temperatures, both translational and internal. Some differences in this coupling may need to be addressed in the future, such as the strongly non-linear behavior of the nonequilibrium reaction rate with vibrational temperature in the widely used Park's reaction model, versus the nearly linear shape for all state-specific approaches. Differences in molecule-molecule versus the molecule-atom vibrational coupling may also require some attention. The impact of the numerical approach on species mole fractions was found to be more significant in oxygen than in nitrogen.

Analysis of vibrational level populations in the strongly thermally nonequilibrium region show the profound impact that the choice of the numerical approach and model has on the population ratios, and thus vibrational temperatures inferred from such ratios. The difference in the absorption coefficients calculated by a temperature-based NEQAIR code using vibrational temperatures inferred from the populations of levels 4 and 6, computed by different state-specific and kinetic approaches, is found to exceed an order of magnitude. This may significantly complicate model validation when comparing to measured temperatures, and may also require a state-specific spectral code to be used when comparing computed and measured absorption spectra.

VI. Acknowledgments

The work at AFRL at was supported by the Air Force Office of Scientific Research (Program Officers Dr. Ivett Leyva and Dr. Sarah Popkin). The work of O. Kunova and E. Kustova was supported by the Russian Science Foundation, project 19-11-00041.

References

- [1] Holloway, M. E., Hanquist, K. M., and Boyd, I. D., "Assessment of Thermochemistry Modeling for Hypersonic Flow over a Double Cone," *Journal of Thermophysics and Heat Transfer*, Vol. 34, No. 3, 2020, p. 538–547. <https://doi.org/10.2514/1.T5792>.
- [2] Gimelshein, S., and Wysong, I., "Nonequilibrium air flow predictions with a high-fidelity direct simulation Monte Carlo approach," *Physical Review Fluids*, Vol. 4, No. 3, 2019, p. 033405. <https://doi.org/10.1103/PHYSREVFLUIDS.4.033405>.
- [3] Hornung, H., and Leyva, I., "Sonic Line and Shock Detachment in Hypervelocity Cone Flow," *IUTAM Symposium Transsonicum IV. Fluid Mechanics and its Application*, Vol. 73, edited by S. H., Springer, Dordrecht, Germany, 2003, pp. 381–386. https://doi.org/10.1007/978-94-010-0017-8_56.
- [4] Karl, S., Martinez-Schramm, J., and Hannemann, K., "High enthalpy cylinder flow in HEG: a basis for CFD validation," *AIAA Paper*, AIAA, Reston, VA, 2003, pp. 2003–4252. <https://doi.org/10.2514/6.2003-4252>.

- [5] Holden, M., MacLean, M., Wadhams, T., and Dufrene, A., "Measurements of Real Gas Effects on Regions of Laminar Shock Wave/Boundary Layer Interaction in Hypervelocity Flows for Blind Code Validation Studies," *AIAA Paper*, AIAA, Reston, VA, 2013, pp. 2013–2837. <https://doi.org/10.2514/6.2013-2837>.
- [6] Ibraguimova, L., Sergievskaya, A., Levashov, V., Shatalov, O., Tunik, Y., and Zabelinskii, I., "Investigation of oxygen dissociation and vibrational relaxation at temperatures 4000–10800 K," *J. Chemical Physics*, Vol. 139, No. 3, 2013, p. 034317. <https://doi.org/10.1063/1.4813070>.
- [7] Candler, G., "Rate effects in hypersonic flows," *Annual Review of Fluid Mechanics*, Vol. 51, 2019, pp. 379–402. <https://doi.org/10.1146/annurev-fluid-010518-040258>.
- [8] Cortesi, A., Constantine, P., Magin, T., and Congedo, P., "Forward and backward uncertainty quantification with active subspaces: application to hypersonic flows around a cylinder," *INRIA Research Report*, Vol. 9097, INRIA, Paris, France, 2017, pp. 1–41.
- [9] Ray, J., Kieweg, S., Dinzl, D., Carnes, B., Weirs, V., Freno, B., M., H., T., S., I., N., and Candler, G. V., "Estimation of inflow uncertainties in laminar hypersonic double-cone experiments," *AIAA J.*, Vol. 58, No. 10, 2020, pp. 4461–4474. <https://doi.org/10.2514/1.J059033>.
- [10] Li, Z., Parsons, N., and Levin, D., "A study of internal energy relaxation in shocks using molecular dynamics based models," *J. Chem. Phys.*, Vol. 143, No. 145, 2015, p. 144501. <https://doi.org/10.1063/1.4931107>.
- [11] Luo, H., Kulakhmetov, M., and Alexeenko, A., "Ab initio state-specific $N_2 + O$ dissociation and exchange modeling for molecular simulations," *J. Chem. Phys.*, Vol. 146, No. 7, 2017, p. 074303. <https://doi.org/10.1063/1.4975770>.
- [12] Streicher, J., Krish, A., and Hanson, R., "Shock-Tube Measurements of Vibrational Relaxation Times in Oxygen and Nitrogen Mixtures Using Ultraviolet Laser Absorption Spectroscopy," *AIAA Paper*, AIAA, Reston, VA, 2020, pp. 2020–1940. <https://doi.org/10.2514/6.2020-1940>.
- [13] Hanquist, K., Chaudhry, R., Boyd, I., Streicher, J., Krish, A., and Hanson, R., "Detailed Thermochemical Modeling of O_2 -Ar in Reflected Shock Tube Flows," *AIAA Paper*, AIAA, Reston, VA, 2020, pp. 2020–3275. <https://doi.org/10.2514/6.2020-3275>.
- [14] Streicher, J., Krish, A., and Hanson, R., "Vibrational relaxation time measurements in shock-heated oxygen and air from 2000 K to 9000 K using ultraviolet laser absorption," *Phys. Fluids*, Vol. 32, No. 8, 2020, p. 086101. <https://doi.org/10.1063/5.0015890>.
- [15] Streicher, J. W., Krish, A., Hanson, R. K., Hanquist, K. M., Chaudhry, R. S., and Boyd, I. D., "Shock-tube measurements of coupled vibration-dissociation time-histories and rate parameters in oxygen and argon mixtures from 5,000-10,000 K," *Physics of Fluids*, Vol. 32, No. 7, 2020. <https://doi.org/10.1063/5.0012426>, URL <https://doi.org/10.1063/5.0012426>.
- [16] McGilvray, M., Doherty, L., Morgan, R., and Gildfind, D., "T6: the Oxford University Stalker tunnel," *AIAA Paper*, AIAA, Reston, VA, 2015, pp. 2015–3545. <https://doi.org/10.2514/6.2017-3545>.

- [17] Leibowitz, M., "Hypervelocity Shock Tunnel Studies of Blunt Body Aerothermodynamics in Carbon Dioxide for Mars Entry," Ph.D. thesis, California Institute of Technology, 2020. <https://doi.org/10.7907/chyn-ea06>.
- [18] Gimelshein, S., and Wysong, I., "Hypersonic non-equilibrium comparison cases," *AIP Conference Proceedings*, 2132, Vol. 1, AIP, 2019, p. 100008. <https://doi.org/10.1063/1.5119603>.
- [19] Olthoff, J., and Greenberg, K., "The Gaseous Electronics Conference RF Reference Cell - An Introduction," *J. Res. Natl. Inst. Stand. Technol.*, Vol. 100, 1995, p. 327. <https://doi.org/10.6028/jres.100.025>.
- [20] Gallis, M., Torczynski, J., Plimpton, S., Rader, D., and Koehler, T., "Direct Simulation Monte Carlo: The Quest for Speed," *AIP Conf. Proc.*, Vol. 1628, AIP, 2014, p. 27. <https://doi.org/10.1063/1.4902571>.
- [21] Ivanov, M., Markelov, G., and Gimelshein, S., "Statistical simulation of the transition between regular and Mach reflection in steady flows," *Computers and Mathematics with Applications*, Vol. 35, No. 1–2, 1998, pp. 113–126. [https://doi.org/10.1016/S0898-1221\(97\)00262-9](https://doi.org/10.1016/S0898-1221(97)00262-9).
- [22] Nompelis, I., Drayna, T., and Candler, G., "A parallel unstructured implicit solver for hypersonic reacting flow simulation," *AIAA Paper*, AIAA, Reston, VA, 2005, pp. 2005–4867. <https://doi.org/10.2514/6.2005-4867>.
- [23] Kustova, E. V., Savelev, A. S., and Kunova, O. V., "Rate coefficients of exchange reactions accounting for vibrational excitation of reagents and products," *AIP Conf. Proc.*, Vol. 1959, AIP, 2018, p. 060010. <https://doi.org/10.1063/1.5034671>.
- [24] Borgnakke, C., and Larsen, P., "Statistical Collision Model for Monte Carlo Simulation of Polyatomic Gas Mixture," *J. Comp. Physics*, Vol. 18, 1975, pp. 405–420. [https://doi.org/10.1016/0021-9991\(75\)90094-7](https://doi.org/10.1016/0021-9991(75)90094-7).
- [25] Adamovich, I., and Rich, J., "Three-dimensional nonperturbative analytic model of vibrational energy transfer in atom-molecule collisions," *J. Chem. Phys.*, Vol. 109, No. 18, 1998, pp. 7711–7724. <https://doi.org/10.1063/1.477417>.
- [26] Adamovich, I., "Three-dimensional analytic model of vibrational energy transfer in molecule-molecule collisions," *AIAA Journal*, Vol. 39, No. 2001, 2001, pp. 1916–1925. <https://doi.org/10.2514/2.1181>.
- [27] Bird, G. A., *Molecular Gas Dynamics and the Direct Simulation of Gas Flows*, Clarendon Press, Oxford, England, UK, 1994.
- [28] Koura, K., "A set of model cross sections for the Monte Carlo simulation of rarefied real gases: Atom-diatom collisions," *Phys. Fluids*, Vol. 6, No. 10, 1994, pp. 3473–3486. <https://doi.org/10.1063/1.868404>.
- [29] Park, C., "Assessment of two-temperature kinetic model for ionizing air," *J. Thermophys. Heat Transf.*, Vol. 3, No. 3, 1989, pp. 233–244. <https://doi.org/10.2514/3.28771>.
- [30] Chaudhry, R., Boyd, I., Torres, E., Schwartzentruber, T., and Candler, G., "Implementation of a Chemical Kinetics Model for Hypersonic Flows in Air for High-Performance CFD," *AIAA Paper*, AIAA, Reston, VA, 2020, pp. 2020–2191. <https://doi.org/10.2514/6.2020-2191>.

- [31] Loukhovitski, B., and Starik, A., "Modeling of vibration-electronic-chemistry coupling in the atomic-molecular oxygen system," *Chemical Physics*, Vol. 360, No. 1-3, 2009, p. 18026. <https://doi.org/10.1016/j.chemphys.2009.04.003>.
- [32] Andrienko, D., and Boyd, I., "Master equation simulation of O₂-N₂ collisions on an ab-initio potential energy surface," *AIAA Paper*, AIAA, Reston, VA, 2017, pp. 2017–3163. <https://doi.org/10.2514/6.2017-3163>.
- [33] Bonelli, F., Tuttafesta, M., Colonna, G., Cutrone, L., and Pascazio, G., "An MPI-CUDA approach for hypersonic flows with detailed state-to-state air kinetics using a GPU cluster," *Computer Physics Communications*, Vol. 219, 2017, pp. 178–195. <https://doi.org/10.1016/j.cpc.2017.05.019>.
- [34] Venturi, S., Sharma, M., Lopez, B., and Panesi, M., "Data-Inspired and Physics-Driven Model Reduction for Dissociation: Application to the O₂+O System," *Journal of Physical Chemistry A*, Vol. 124, No. 41, 2020, pp. 8359–8372. <https://doi.org/10.1021/acs.jpca.0c04516>.
- [35] Josyula, E., Suchyta, C. J., Vedula, P., and Burt, J. M., "Multiquantum Transitions in Oxygen and Nitrogen Molecules in Hypersonic Nonequilibrium Flows," *Journal of Thermophysics and Heat Transfer*, Vol. 33, No. 2, 2019, pp. 378–391. <https://doi.org/10.2514/1.T5444>.
- [36] Grover, M. S., Suchyta, C. J., and Josyula, E., "Ab Initio Based Rate Coefficients for Two-Temperature Nonequilibrium Models in Hypersonic Blunt Body Flow," *AIAA Scitech 2019 Forum*, AIAA Paper 2019-0790, 2019. <https://doi.org/10.2514/6.2019-0790>.
- [37] Kulakhmetov, M., Gallis, M., and Alexeenko, A., "Ab initio-informed maximum entropy modeling of rovibrational relaxation and state-specific dissociation with application to the O₂ + O system," *J. Chem. Phys.*, Vol. 144, No. 17, 2016, p. 174302. <https://doi.org/10.1063/1.4947590>.
- [38] Gimelshein, N., Gimelshein, S., and Levin, D., "Vibrational relaxation rates in the direct simulation Monte Carlo method," *Phys. Fluids*, Vol. 14, No. 12, 2002, pp. 4452–4455. <https://doi.org/10.1063/1.1517297>.
- [39] Park, C., "Problems of Rate Chemistry in the Flight Regimes of Aeroassisted Orbital Transfer Vehicles," *Prog. Astronaut. Aeronaut.*, Vol. 6, 1985, pp. 511–537. <https://doi.org/10.2514/6.1984-1730>.
- [40] Gimelshein, S., and Wysong, I., "DSMC modeling of flows with recombination reactions," *Phys. Fluids*, Vol. 29, No. 6, 2017, p. 067106. <https://doi.org/10.1063/1.49865297>.
- [41] Bird, G., "Monte Carlo simulations in an engineering context," *Prog. Astronaut. Aeronaut.*, Vol. 74, 1981, pp. 239–255. <https://doi.org/10.2514/5.9781600865480.0239.0255>.
- [42] McBride, B., Zehe, M., and Gordon, S., "NASA Glenn Coefficients for Calculating Thermodynamic Properties of Individual Species," *NASA Report*, 2002, pp. NASA/TP?2002–211556.
- [43] Andrienko, D. A., and Boyd, I. D., "Rovibrational energy transfer and dissociation in O₂-O collisions," *The Journal of chemical physics*, Vol. 144, No. 10, 2016, p. 104301.

- [44] Paukku, Y., Varga, Z., and Truhlar, D. G., "Potential energy surface of triplet O₄," *The Journal of chemical physics*, Vol. 148, No. 12, 2018, p. 124314. <https://doi.org/10.1063/1.5017489>.
- [45] Varga, Z., Paukku, Y., and Truhlar, D. G., "Potential energy surfaces for O + O₂ collisions," *The Journal of chemical physics*, Vol. 147, No. 15, 2017, p. 154312. <https://doi.org/10.1063/1.4997169>.
- [46] Jaffe, R., Schwenke, D., Chaban, G., and Huo, W., "Vibrational and rotational excitation and relaxation of nitrogen from accurate theoretical calculations," *AIAA Paper*, AIAA, Reston, VA, 2008, pp. 2008–1208. <https://doi.org/10.2514/6.2008-1208>.
- [47] Bender, J. D., Valentini, P., Nompelis, I., Paukku, Y., Varga, Z., Truhlar, D. G., Schwartzentruber, T., and Candler, G. V., "An improved potential energy surface and multi-temperature quasiclassical trajectory calculations of N₂ + N₂ dissociation reactions," *The Journal of Chemical Physics*, Vol. 143, No. 5, 2015, p. 054304. <https://doi.org/10.1063/1.4927571>.
- [48] Campoli, L., Kunova, O., Kustova, E., and Melnik, M., "Models validation and code profiling in state-to-state simulations of shock heated air flows," *Acta Astronautica*, Vol. 175, 2020, pp. 493–509. <https://doi.org/10.1016/j.actaastro.2020.06.008>.
- [49] Adamovich, I., Macheret, S., Rich, J., and Treanor, C., "Vibrational energy transfer rates using a forced harmonic oscillator model," *J. Thermophys. Heat Transfer.*, Vol. 12, 1998, p. 57–65. <https://doi.org/10.2514/2.6302>.
- [50] Kunova, O., Kustova, E., and Savelev, A., "Generalized Treanor–Marrone model for state-specific dissociation rate coefficients," *Chem. Phys. Lett.*, Vol. 659, 2016, pp. 80–87. <https://doi.org/10.1016/j.cplett.2016.07.006>.
- [51] Esposito, F., Armenise, I., and Capitelli, M., "N-N₂ state to state vibrational-relaxation and dissociation rates based on quasiclassical calculations," *Chem. Phys.*, Vol. 331, No. 1, 2006, pp. 1–8. <https://doi.org/10.1016/j.chemphys.2006.09.035>.
- [52] Esposito, F., Armenise, I., Capitta, G., and Capitelli, M., "O-O₂ state-to-state vibrational relaxation and dissociation rates based on quasiclassical calculations," *Chem. Phys.*, Vol. 351, No. 1–3, 2008, pp. 91–98. <https://doi.org/10.1016/j.chemphys.2008.04.004>.
- [53] Scanlon, T., White, C., Borg, M., Palharini, R., Farbar, E., Boyd, I., Reese, J., and Brown, R., "Open-source direct simulation Monte Carlo chemistry modeling for hypersonic flows," *AIAA Journal*, Vol. 53, No. 6, 2015, pp. 1670–1680. <https://doi.org/10.2514/1.J053370>.
- [54] Economon, T. D., Palacios, F., Copeland, S. R., Lukaczyk, T. W., and Alonso, J. J., "SU2: An Open-Source Suite for Multiphysics Simulation and Design," *AIAA Journal*, Vol. 54, No. 3, 2016, pp. 828–846. <https://doi.org/10.2514/1.J053813>.
- [55] Millikan, R., and White, D., "Systematics of Vibrational Relaxation," *J. Chem. Phys.*, Vol. 39, 1963, pp. 3209–3213. <https://doi.org/10.1063/1.1734182>.
- [56] Park, C., "Assessment of two-temperature kinetic model for ionizing air," *Journal of Thermophysics and Heat Transfer*, Vol. 3, No. 3, 1989, pp. 233–244. <https://doi.org/10.2514/3.28771>.
- [57] Scoggins, J. B., "Development of numerical methods and study of coupled flow, radiation, and ablation phenomena for atmospheric entry," Ph.D. thesis, von Karman Institute for Fluid Dynamics, 2017.

- [58] Scalabrin, L. C., “Numerical Simulation of Weakly Ionized Hypersonic Flow over Reentry Capsules,” Ph.D. thesis, University of Michigan, Ann Arbor, 2007.
- [59] Martin, A., Scalabrin, L. C., and Boyd, I. D., “High performance modeling of atmospheric re-entry vehicles,” *Journal of Physics: Conference Series*, Vol. 341, 2012, pp. 1–12. <https://doi.org/10.1088/1742-6596/341/1/012002>.
- [60] Park, C., *Nonequilibrium Hypersonic Aerothermodynamics*, Wiley, New York, 1990.
- [61] Capitelli, M., Gorse, C., Longo, S., and Giordano, “Collision Integrals of High-Temperature Air Species,” *J. Thermophys. Heat Transf.*, Vol. 14, No. 2, 2000, pp. 259–268. <https://doi.org/10.2514/2.6517>.
- [62] Gimelshein, S., Boyd, I., and Ivanov, M., “DSMC Modeling of Vibration-Translation Energy Transfer in Hypersonic Rarefied Flows,” *AIAA Paper 99-3451*, June 1999. <https://doi.org/10.2514/6.1999-3451>.
- [63] Gimelshein, S., Wysong, I., and Adamovich, I., “Application of the 3D Forced Harmonic Oscillator Model in the DSMC Method,” *J. Thermophys. Heat Transf.*, Vol. 32, No. 4, 2018, pp. 882–891. <https://doi.org/10.2514/1.T5228>.
- [64] Bergemann, F., and Boyd, I., “DSMC simulation of inelastic collisions using the Borgnakke-Larsen method extended to discrete distributions of vibrational energy,” *Rarefied Gas Dynamics: Theory and Simulations*, Progress in Astronautics and Aeronautics, Vol. 32, edited by B. D. Shizgal and D. P. Weaver, AIAA, Washington, DC, 1996, pp. 174–183.
- [65] Gimelshein, S., and Wysong, I., “Modeling of vibration-vibration energy transfer in the DSMC Method,” *J. Thermophys. Heat Transf.*, Vol. 32, No. 31, 2018, pp. 781–788. <https://doi.org/10.2514/1.T5331>.
- [66] Wadsworth, D., and Wysong, I., “Vibrational favoring effect in DSMC dissociation models,” *Phys. Fluids*, Vol. 9, No. 12, 1997, pp. 3873–3884. <https://doi.org/10.1063/1.869487>.
- [67] Chaudhry, R., Grover, M., Bender, J., Schwartztruber, T., and Candler, G., “Quasiclassical Trajectory Analysis of Oxygen Dissociation via O_2 , O, and N_2 ,” *AIAA Paper*, AIAA, Reston, VA, 2018, pp. 2018–0237. <https://doi.org/10.2514/6.2018-0237>.
- [68] Nagnibeda, E., and Kustova, E., *Nonequilibrium Reacting Gas Flows. Kinetic Theory of Transport and Relaxation Processes*, Springer-Verlag, Berlin, Heidelberg, 2009. <https://doi.org/10.1007/978-3-642-01390-4>.
- [69] Panesi, M., A. Munafò, Magin, T. E., and Jaffe, R. L., “Nonequilibrium shock-heated nitrogen flows using a rovibrational state-to-state method,” *Phys. Rev. E*, Vol. 90, 2014, p. 013009. <https://doi.org/10.1103/PhysRevE.90.013009>.
- [70] Armenise, I., Esposito, F., and Capitelli, M., “Dissociation–recombination models in hypersonic boundary layer flows,” *Chemical Physics*, Vol. 336, No. 1, 2007, pp. 83–90. <https://doi.org/10.1016/j.chemphys.2007.05.015>.
- [71] Scoggins, J. B., Leroy, V., Bellas-Chatzigeorgis, G., Dias, B., and Magin, T. E., “Mutation++: MUlticomponent Thermodynamic And Transport properties for IONized gases in C++,” *SoftwareX*, Vol. 12, 2020, p. 100575. <https://doi.org/https://doi.org/10.1016/j.softx.2020.100575>.

- [72] Liou, M.-S., and Steffen, C. J., “A New Flux Splitting Scheme,” *Journal of Computational Physics*, Vol. 107, No. 1, 1993, pp. 23–39. <https://doi.org/10.1006/jcph.1993.1122>.
- [73] MacCormack, R. W., and Candler, G. V., “The solution of the Navier-Stokes equations using Gauss-Seidel line relaxation,” *Computers & Fluids*, Vol. 17, No. 1, 1989, pp. 135 – 150. [https://doi.org/10.1016/0045-7930\(89\)90012-1](https://doi.org/10.1016/0045-7930(89)90012-1).
- [74] Landau, L., and Teller, E., “Theory of sound dispersion,” *Physik Zeitschrift der Sowjetunion*, Vol. 10, 1936, pp. 34–38.
- [75] Park, C., “Review of chemical-kinetic problems of future NASA missions. I - Earth entries,” *Journal of Thermophysics and Heat Transfer*, Vol. 7, No. 3, 1993, pp. 385–398. <https://doi.org/10.2514/3.431>.
- [76] Park, C., Jaffe, R. L., and Partridge, H., “Chemical-Kinetic Parameters of Hyperbolic Earth Entry,” *Journal of Thermophysics and Heat Transfer*, Vol. 15, No. 1, 2001, pp. 76–90. <https://doi.org/10.2514/2.6582>.
- [77] Candler, G. V., and MacCormack, R. W., “Computation of Weakly Ionized Hypersonic Flows in Thermochemical Nonequilibrium,” *Journal of Thermophysics and Heat Transfer*, Vol. 5, No. 3, 1991, pp. 266–273. <https://doi.org/10.2514/3.260>.
- [78] Lee, J.-H., “Basic governing equations for the flight regimes of aeroassisted orbital transfer vehicles,” *19th AIAA Thermophysics Conference*, AIAA Paper 1984-1729, Snowmass, CO, 1984, pp. 1–18. <https://doi.org/10.2514/6.1984-1729>.
- [79] Gurvich, L. V., Veits, I. V., and Alcock, C. B., *Thermodynamics properties of individual substances. Volume 1 - Elements O, H/D, T, F, Cl, Br, I, He, Ne, Ar, Kr, Xe, Rn, S, N, P, and their compounds. Part 1 - Methods and computation.*, 4th ed., Hemisphere Publishing Corporation, 1989.
- [80] Gurvich, L. V., Veits, I. V., and Alcock, C. B., *Thermodynamics properties of individual substances. Volume 1 - Elements O, H/D, T, F, Cl, Br, I, He, Ne, Ar, Kr, Xe, Rn, S, N, P, and their compounds. Part 2 - Methods and computation.*, 4th ed., Hemisphere Publishing Corporation, 1989.
- [81] Rich, J., and Treanor, C., “Vibrational relaxation in gas dynamic flows,” *Annual Review of Fluid Mechanics*, Vol. 2, 1970, pp. 355–396. <https://doi.org/10.1146/annurev.fl.02.010170.002035>.
- [82] Gimelshein, S., Ivanov, M., Markelov, G., and Gorbachev, Y., “Statistical simulation of nonequilibrium rarefied flows with quasiclassical vibrational energy transfer models,” *Journal of Thermophysics and Heat Transfer*, Vol. 12, No. 4, 1998, pp. 489–495. <https://doi.org/10.2514/6.1997-2585>.
- [83] Park, C., “Rotational relaxation of N₂ behind a strong shock wave,” *J. Thermophys. Heat Transfer*, Vol. 18, No. 4, 2004, pp. 527–533. <https://doi.org/10.2514/1.11442>.
- [84] Herzfeld, K., and Litovitz, T., *Absorption and dispersion of ultrasonic waves*, Academic Press, New York, NY, 1959.
- [85] Grover, M., Schwartzentruber, T., Varga, Z., and Truhlar, D., “Dynamics of vibrational energy excitation and dissociation in oxygen from direct molecular simulation,” *AIAA Paper*, AIAA, Reston, VA, 2018, pp. 2018–0238. <https://doi.org/10.2514/6.2018-0238>.

- [86] Varandas, A., and Pais, A., "A realistic double many-body expansion (DMBE) potential energy surface for ground-state O₃ from a multiproperty fit to ab initio calculations, and to experimental spectroscopic, inelastic scattering, and kinetic isotope thermal rate data," *Mol. Phys.*, Vol. 65, 1988, pp. 843–860. [https://doi.org/10.1016/S1386-1425\(01\)00661-8](https://doi.org/10.1016/S1386-1425(01)00661-8).
- [87] Park, C., "Two-temperature interpretation of dissociation rate data for N₂ and O₂," *AIAA Paper*, AIAA, Reston, VA, 1988, pp. 88–0458. <https://doi.org/10.2514/6.1988-0458>.
- [88] Valentini, P., Schwartzentruber, T., Bender, J., Nompelis, I., and Candler, G., "Direct molecular simulation of nitrogen dissociation based on an ab initio potential energy surface," *Physics of Fluids*, Vol. 27, 2015, p. 086102. <https://doi.org/10.1063/1.4929394>.
- [89] Truhlar, D. G., and Muckerman, J. T., "Reactive scattering cross sections III: Quasiclassical and semiclassical methods," *Atom-Molecule Collision Theory*, Springer, 1979, pp. 505–566. https://doi.org/10.1007/978-1-4613-2913-8_16.
- [90] Billing, G. D., "The semiclassical coupled states method," *The Journal of Chemical Physics*, Vol. 65, No. 1, 1976, pp. 1–6. <https://doi.org/10.1063/1.432796>.
- [91] Gimelshein, S., Wysong, I., Bykova, N., O.P., S., and I.E., Z., "Improved Analysis of O₂ Ultraviolet Absorption Spectra Under Nonequilibrium Shock Conditions," *AIAA Journal*, Vol. 58, No. 10, 2020. <https://doi.org/10.2514/1.J058961>.
- [92] Neitzel, K. J., Andrienko, D. A., and Boyd, I. D., "Aerothermochemical Nonequilibrium Modeling for Oxygen Flows," *Journal of Thermophysics and Heat Transfer*, Vol. 31, No. 3, 2017, pp. 634–645. <https://doi.org/10.2514/1.T4962>.
- [93] Gimelshein, S., "Particle Modeling of Reflected Shock Waves," *J. Thermophysics and Heat Transfer*, Accepted for publication, 2020.
- [94] Liechty, D., and Lewis, M., "Treatment of Electronic Energy Level Transition and Ionization Following the Particle-Based Chemistry Model," *AIAA Paper*, AIAA, Reston, VA, 2010, pp. 2010–0449. <https://doi.org/10.2514/6.2010-0449>.
- [95] Kunova, O., Kustova, E., Mekhonoshina, M., and Shoev, G., "Numerical simulation of coupled state-to-state kinetics and heat transfer in viscous non-equilibrium flows," *AIP Conference Proceedings*, Vol. 1786, 2016, p. 070012. <https://doi.org/10.1063/1.4967588>.
- [96] Andrienko, D., and Boyd, I., "State-specific dissociation in O₂-O₂ collisions by quasiclassical trajectory method," *Chemical Physics*, Vol. 491, 2017, pp. 74–81.
- [97] Varandas, A., and Llanio-Trujillo, J., "Dynamics of O+O₃ reaction on a new potential energy surface for ground-triplet tetraoxygen: spectator bond mechanism revisited," *J. Theor. Comput. Chem.*, Vol. 1, No. 1, 2002, pp. 31–43. <https://doi.org/10.1142/S021963360200018X>.
- [98] Cruden, B., and Brandis, A., "Updates to Neqair radiation solver," *NASA Technical Report*, NASA, Moffet Field, CA, 2014, pp. ARC–E–DAA–TN19271.

- [99] Laux, C., Spence, T., Kruger, C., and Zare, R., “Optical diagnostics of atmospheric pressure air plasmas,” *Plasma Sources Sci. Technol.*, Vol. 12, 2003, pp. 125–138. <https://doi.org/10.1088/0963-0252/12/2/301>.
- [100] Bykova, N., and Kuznetsova, L., “Study of the Absorption Characteristics of Molecular Oxygen in the Schumann-Runge System at High Temperatures: I. Calculations of Absorption Spectra,” *Optics and Spectroscopy*, Vol. 105, No. 5, 2008, pp. 668–673. <https://doi.org/10.1134/S0030400X08110040>.